Check for updates

ADVANCED MATERIALS
www.advmat.de

Reaction Mechanisms and Kinetics of Nanozymes: Insights from Theory and Computation

*Xiaomei Shen, Zhenzhen Wang, Xuejiao J. Gao, and Xingfa Gao**

"Nanozymes" usually refers to inorganic nanomaterials with enzyme-like catalytic activities. The research into nanozymes is one of the hot topics on the horizon of interdisciplinary science involving materials, chemistry, and biology. Although great progress has been made in the design, synthesis, characterization, and application of nanozymes, the study of the underlying microscopic mechanisms and kinetics is still not straightforward. Density functional theory (DFT) calculations compute the potential energy surfaces along the reaction coordinates for chemical reactions, which can give atomistic-level insights into the micro-mechanisms and kinetics for nanozymes. Therefore, DFT calculations have been playing an increasingly important role in exploring the mechanisms and kinetics for nanozymes in the past years. The calculations either predict the microscopic details for the catalytic processes to compliment the experiments or further develop theoretical models to depict the physicochemical rules. In this review, the corresponding research progress is summarized. Particularly, the review focuses on the computational studies that closely interplay with the experiments. The relevant experimental results without DFT calculations will be also briefly discussed to offer a historic overview of how the computations promote the understanding of the microscopic mechanisms and kinetics of nanozymes.

1. Introduction

The term "nanozyme" was coinded by Manea et al. in 2004 to describe the ribonidase-like catalytic activity of the azacrown modified gold nanoparticles.[1] Since the pioneering work that reported the intrinsic peroxidase-like activity of Fe_3O_4 nanoparticles in 2007,[2] nanozymes have attracted much research interest. Nanozymes normally denote inorganic nanomaterials having enzyme-like catalytic activities.[3] Compared to enzymes, the nanozymes are usually easier to prepare, store, and transport. Because they are more stable and have larger specific areas with more catalytic centers, they can work more efficiently in the severe environments.[2,4] They can also inherit the fascinating optical, electrical, and magnetic properties of nanomaterials, which are not owned by enzymes.[5] Therefore, they are promising to serve as the multifunctional, artificial enzymes. The research of nanozyme has become one of the hottest topics on the horizon of interdisciplinary science involving materials, chemistry, biology, and medicine.

In the past years, great progress has been made in the nanozyme research. Hundreds of nanozymes based on carbons, metals, metal oxides, and their mixtures have been fabricated. They mimic a variety of enzymes, which mainly include the members of the oxidordeuctase family such as peroxidases,[6] catalases,[7] oxidases,[8] and superoxide dismutase (SOD).[9] Those mimicking the activities of the hydrolase[10] and dehydrogenase[11] families have also been discovered. The potential of nanozymes to replace the corresponding natural enzymes in many applications in the fields of diagnosis,[12] therapy,[13] and environmental restoration[14] has been established. A number of excellent review papers, which comprehensively discuss the progress achieved in the research of the synthesis, characterization, classification, and application of nanozymes, have been published in the past years.[15]

Despite the progress, a systematic and in-depth understanding of the catalytic activities of nanozymes is still difficult. It is particularly challenging to predict the enzyme-like activities of nanomaterials or design new nanozymes with the desired activities prior to experiments, which is requested by the practical applications. As far as the chemistry is concerned, nanozymes are the nanomaterial-based catalysts. Without expectation, the experimentally observed catalytic activities of nanozymes are the overall consequences of the microscopic reactions occurring on the materials surfaces (**Figure 1**a). Therefore, the microscopic mechanisms and kinetics of the nanozyme catalyses and the rule of how the catalyses vary with the structures and electronic properties of the materials are the core knowledge, which is crucial for the understanding and predictive design of nanozyme activities.

Unfortunately, the characterization of the micro-mechanisms and kinetics for nanozymes is not straightforward. The obstacles mainly exist in two aspects: first, most nanozymes are

X. Shen, X. J. Gao
College of Chemistry and Chemical Engineering
Jiangxi Normal University
Nanchang 330022, China
Z. Wang, X. Gao
Laboratory of Theoretical and Computational Nanoscience
National Center for Nanoscience and Technology
Chinese Academy of Sciences
Beijing 100190, China
E-mail: gaoxf@nanoctr.cn

The ORCID identification number(s) for the author(s) of this article can be found under https://doi.org/10.1002/adma.202211151

DOI: 10.1002/adma.202211151

 © 2023 Wiley-VCH GmbH

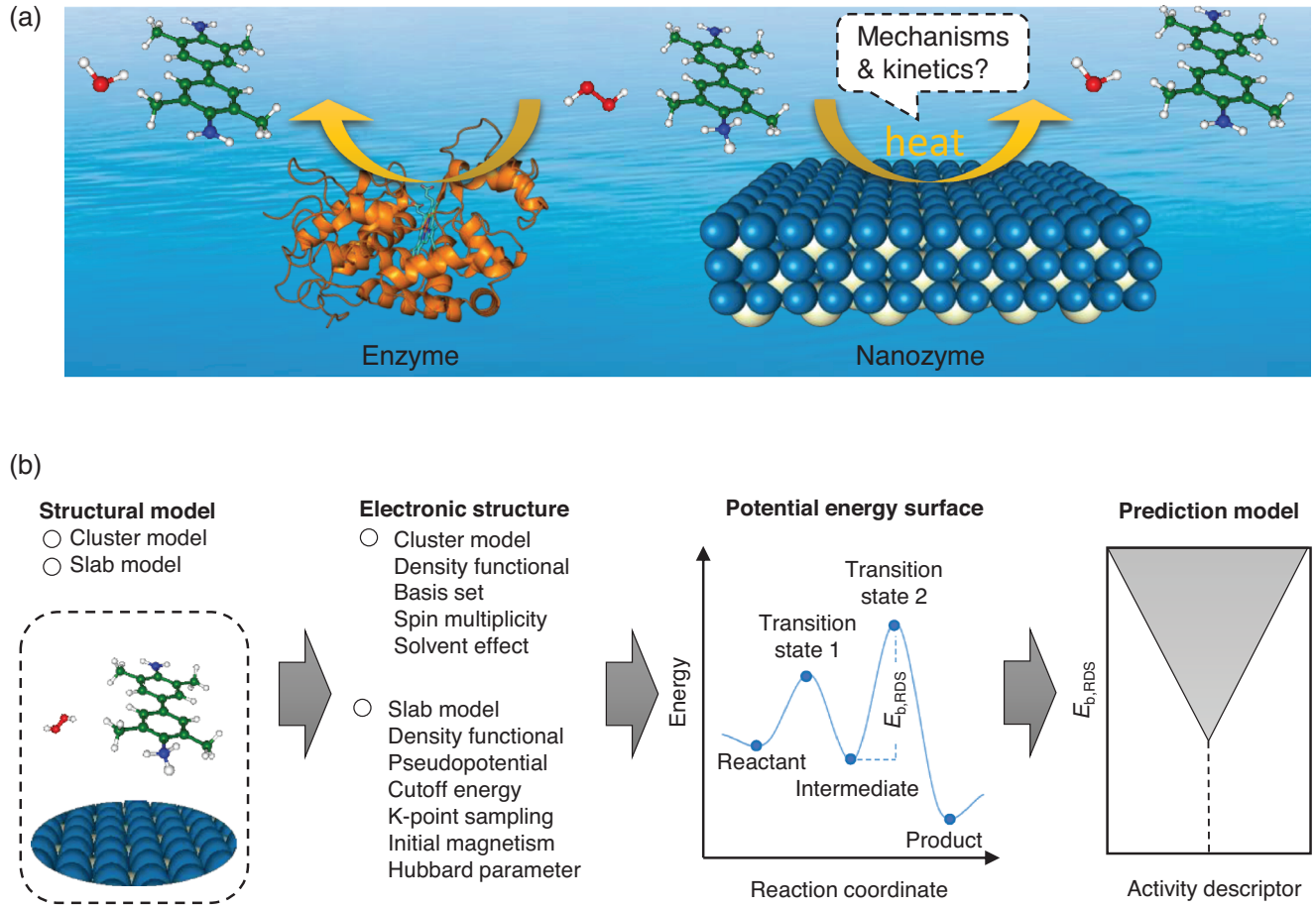

Figure 1. DFT study of nanozymes. a) The comparison between the catalysis of an enzyme and that of a nanozyme, suggesting nanozymes to be the nanomaterials-based heterogeneous catalysts. b) Procedures of DFT studies of the mechanisms, kinetics, and prediction models of nanozymes.

amorphous nanoparticles with inhomogeneous sizes, shapes, and conformations, whose precise atomic compositions, crystal structures, and exposed facets are hard to characterize;[16] second, nanozymes work in complex aqueous conditions, in which the exact species of the transient intermediates involved in the catalytic cycles are hard to detect.[17] These obstacles have severely hindered the convincible survey of the micro-mechanisms and kinetics of nanozymes.

Density functional theory (DFT) calculations can compute the potential energy surfaces along the reaction coordinates for chemical reactions, giving atomistic-level insights into the micro-mechanisms and kinetics. Because it bridges the gap between the frontier experiments and fundamental theories for reactions, this approach has been widely applied to study the reaction mechanisms and kinetics for nearly all branches of chemistry.[18] The computational approach has also been applied in the nanozyme research.[19] More and more papers published on nanozymes in the recent years have involved DFT calculations. The calculations either predict microscopic details for the catalytic reactions to compliment the experiments or further develop mathematic models to depict the physicochemical rules underlying the experiments. The results have provided the in-depth understanding of the nanozyme chemistry and the theoretical guidelines for the predictive design of nanozyme activities.

Here, the progress in the research of catalytic mechanisms and kinetics of nanozymes by means of DFT calculations will be reviewed. The studies dealing with the catalytic mechanisms and kinetics without the label of "nanozyme" will be also considered. Particularly, the review will be focused on the computational studies that closely interplay with the experiments. Only computational studies addressing the underlying mechanisms for experiments through some kinds of mutual verification way, will be emphatically referenced. The relevant experimental results without DFT calculations will be briefly discussed to offer a historic overview of how the computations promote the understanding of the microscopic mechanisms and kinetics of nanozymes. The future perspective and challenges on the computational studies of nanozymes will also be included. The scope of this review is different from those publish previously, which are mainly on the syntheses, characterizations, classifications, and applications of nanozymes. This review is expected to help experimentalists better understand the underling mechanisms and kinetics of nanozymes from the microscopic and theoretical points of view, and attract computational chemists to carry out more in-depth and extensive studies on this topic, so as to spark future ideas for designing more stable, efficient, and fascinating nanozymes with potentials in applications prior to experiments.

© 2023 Wiley-VCH GmbH

15214095, 0, Downloaded from https://onlinelibrary.wiley.com/doi/10.1002/adma.202211151 by Eth Zürich Eth-Bibliothek, Wiley Online Library on [11/07/2023]. See the Terms and Conditions (https://onlinelibrary.wiley.com/terms-and-conditions) on Wiley Online Library for rules of use; OA articles are governed by the applicable Creative Commons License

2. Computational Methods

DFT calculations predict reaction mechanisms and kinetics based on the potential energy surfaces of the reaction systems along the reaction coordinates, which are explicit in physics and rigorous in physicochemical principles. Therefore, they are possible to closely interplay with the advanced experimental approaches that are built on the same physicochemical foundations. To perform the calculations for nanozymes, the structure models should be first established. Depending on the materials which the nanozymes are based on, either cluster models or periodic slab models can be built (Figure 1b). The cluster models are usually applicable for molecule-based nanozymes[20] and the slab models are applicable to crystal-based nanozymes.[21] Because the cluster models could invoke the hybrid density functionals with a better computational efficiency, the cluster models have also used for some graphene and metal-organic framework (MOF)-based nanozymes. However, for most of the metal and metal oxide nanozymes in which the atoms form metal or ionic bonds, the periodic slabs are necessary to properly model the global electronic structures and local atomic environments of the systems. With either the cluster models or the slab models, the computations of nanozymes are markedly different from those of natural enzymes. The DFT method is usually sufficient for the computations of nanozymes. In contrast, the combined quantum-mechanics and molecular-mechanics approach is usually necessary for the computations of natural enzymes in order to simulate the function of the large protein scaffolds of enzymes.[22]

The electronic structures as well as the interatomic forces of the structural models will then be calculated. The settings for the calculations following the cluster models are the same as the normal DFT calculations for molecular systems.[20] Typically, the density functionals, basis sets, spin multiplicities, and solvent models of the systems should be defined. If the system contains multiple weak interactions, the dispersion effect needs to be increased. A lot of computational codes such as Gaussian[23] and Gamess[24] are suitable for these calculations. Likewise, the subsequent settings of calculations following the slab models are also the same as the normal DFT calculations for crystal systems.[21] The important settings for the plane wave basis DFT calculations include the setting of the density functionals, pseudopotential, basis set energy cutoff, K-point sampling, and if applicable, the initial magnetisms and Hubbard parameters. Computational codes such as VASP[25] and CASTEP[26] are appropriate for these calculations.

On the basis of the interatomic forces of the model structures, the reactants, transition states, intermediates, and products involved in the reactions can be located using the corresponding geometry optimization algorithms, which form the energy profiles of the catalytic cycle along the reaction coordinates (Figure 1b). The detailed atomic-level mechanisms and kinetics can be obtained by analyzing the energy profiles and the key structures and electronic structures along the reaction coordinates.

Of note, the practical nanozymes usually have amorphous structures and work in the complex aqueous conditions. The precise active centers of the nanozymes in the working environments may be hard to simulate with simple structural models. Such a possible discrepancy between the real catalysts and the computational models may produce "errors" for the calculated results. For example, the water molecules may react with the material surfaces to change the surface morphologies and thus critically influence the surface catalytic activities.[27] The water molecules may also participate in the catalysis by assisting the transfer of hydrogen atoms in the important reaction steps.[28] In these cases, the water molecules should be explicitly considered in the DFT calculations. The water molecules also provide a polar solvating environment, contributing to stabilizing the charged species possibly involved in the catalysis. Although the test calculations suggested that the neglect of this solvent effect did not cause severe systematic errors for some of the nanozymes,[29] its effect on other nanozyme systems is unknown and deserves attention. Furthermore, the insufficient levels of theory used, for example, small basis sets or basis-set cutoff energies, sparse K-point grids, and unreasonable Hubbard parameters, may also introduce errors for the calculations. Therefore, before performing the DFT calculations for a new nanozyme system, it is critical test the accuracy of the models and methods to ensure that they satisfy the requirement of the research purposes.

3. Oxidoreductase-Like Nanozymes

3.1. Peroxidase-Like Nanozymes

3.1.1. Structure–Activity Relationships from Experiments

The typical reaction catalyzed by a peroxidase nanozyme can be written as follows:

$$H_2O_2 + 2TMB + 2H^+ = 2H_2O + 2TMB^+ \quad (1)$$

where TMB is 3,3″,5,5″-tetramethylbenzidine and TMB^+ is its cation, namely, the oxidized form of TMB. TMB is one of the most-commonly used chromogenic substrates of oxidation reactions because of its high sensitivity to the reactions. When TMB is oxidized, the solution color may change from colorless to blue by the one-electron oxidation in the neutral or weak acidic condition or yellow by the two-electron oxidation in the strong acidic condition.[30] For both the one-electron and two-electron oxidations, the UV–vis adsorption spectra suggested that the oxidation products were the complexes consisting of TMB and the cation (TMB^+ or TMB^{2+}).[31] **Figure 2** shows the possible paths for the TMB oxidation in acidic conditions, in which protonation and dehydrogenation are the main reaction processes. Because the protonation of amine and imine does not involve the breaking of any chemical bonds, these processes should be kinetically facile in the acidic conditions. Likewise, the formation of the complexes of the products are also kinetically easy. Therefore, the dehydrogenation processes, for example, the TMB → TMB-dH and TMB-H^+ → TMB^+ steps involving the N–H bond breaking, are usually explored to evaluate whether the whole oxidation reactions are feasible (Figure 2).

Following the pioneering discovery of the Fe_3O_4 nanozyme,[2] many nanomaterials based on metals, metal oxides, carbons, and their hybrids, have been found to possess similar catalytic activities, which can catalyze the reaction of Equation (1) mimicking peroxidases.[32] Various structure–activity relationships have been reported for peroxidase-like catalytic activities of

© 2023 Wiley-VCH GmbH

15214095, 0, Downloaded from https://onlinelibrary.wiley.com/doi/10.1002/adma.202211151 by Eth Zürich Eth-Bibliothek, Wiley Online Library on [11/07/2023]. See the Terms and Conditions (https://onlinelibrary.wiley.com/terms-and-conditions) on Wiley Online Library for rules of use; OA articles are governed by the applicable Creative Commons License

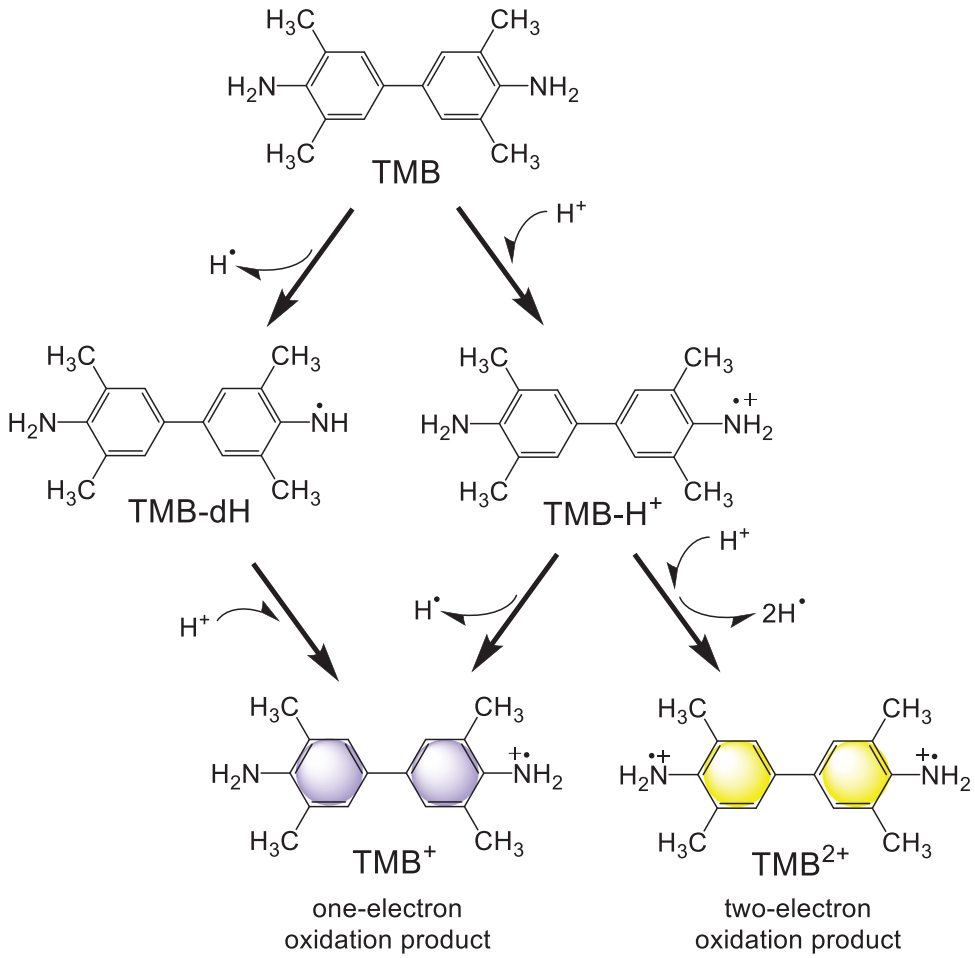

Figure 2. Oxidation of the chromogenic substrate 3,3",5,5"-tetramethylbenzidine (TMB) in acidic conditions. The structures of the oxidation products in the form of complexes are not shown for simplicity. Adapted with permission.[31] Copyright 1997, Elsevier.

nanomaterials. Besides sizes and surface modifications, some other features of nanoparticles, which are summarized in **Table 1**, have been also experimentally demonstrated to critically influence the activity.

Taking one of the mostly studied nanomaterials, nanoceria (i.e., nano-CeO_2), as an example, several features critically influence its catalytic activity. Tian et al. explored that the peroxidase-like activity of nanoceria was morphology dependent and associated with the surface Ce^{3+} fraction and its corresponding oxygen vacancies concentration.[36a] The authors proposed that the surface Ce^{3+} species would function as the active sites of peroxidase-like activity for TMB oxidization in the presence of H_2O_2. Yang et al. further found that the peroxidase-like activity of nanoceria was related to the crystal facets.[36b] The authors synthesized CeO_2 nanorods and nanocubes with the similar concentration of Ce^{3+} and found that the nanorods with (100) facet exhibited higher activity than the nanocubes mainly exposing the (110) facet. Zhao et al. found that the activity was positively relevant to the Ce^{3+}/Ce^{4+} ratio when CeO_2 was dispersed on TiO_2 nanotube.[32d] Yet, Jampaiah et al. found that the activity of Fe-doped CeO_2 nanorods was in direct proportion to surface Ce^{3+} fraction or the adsorbed oxygen (O_β) species.[37a] Guo et al. synthesized nanoceria using the doping of the first row of transition metals, Mn, Fe, Co, Ni, and Cu.[37b] Their experiment indicated that the activity depended on surface oxygen species (O_β) rather than surface Ce^{3+} fraction and that the activity increased with the rise of surface O_β species fraction. Obviously, understanding the mechanisms of the above structure–activity relationship is essential for the further research and development of nanoceria-based peroxidase nanozymes, especially for the forward-looking prediction and design of the activity prior to experiments.

Similar mechanistic questions on structure–activity relationships also exist for other peroxidase nanozymes (Table 1). For example, He et al. found that nanostructures based on AgM bimetallic alloy (M = Au, Pd, Pt) have atomic-composition and morphology dependent activity.[32b] Fan et al. suggested that the histidine modification could highly improve the peroxidase-like catalytic activity.[39b] Cao et al. reported that defect-rich active edges could enhance the peroxidase-like activity of MoS_2.[42] Wang et al. accounted that the coordination number of single Mo sites could regulate the peroxidase-like specificity.[46] Because catalytic activities are intrinsically substantialized by atomistic-level reaction mechanisms and kinetics, the progress on the

© 2023 Wiley-VCH GmbH

15214095, 0, Downloaded from https://onlinelibrary.wiley.com/doi/10.1002/adma.202211151 by Eth Zürich Eth-Bibliothek, Wiley Online Library on [11/07/2023]. See the Terms and Conditions (https://onlinelibrary.wiley.com/terms-and-conditions) on Wiley Online Library for rules of use; OA articles are governed by the applicable Creative Commons License

Table 1. Typical materials features influencing the activities of peroxidase nanozymes.

Nanozymes	Features determining the catalytic activity	References
Noble metals	Exposed facet, morphology, composition, surface modification	[32b,33]
$Au_{40}(S\text{-}Adm)_{22}$ nanocluster	Ligand	[34]
$Au_{24}M_1$ (M = Ag, Au, Zn, Er, Pt, Cu, Cd,) nanocluster	Composition	[35]
Nanoceria	Morphology, Ce^{3+}/Ce^{4+} fraction, oxygen vacancies concentration, surface modification	[32d,36]
Metal doped ceria	Surface Ce^{3+} fraction, surface oxygen species	[37]
V_2O_5	Peroxide complex, crystal facets	[38]
Fe_3O_4	Structural defect, size, modification	[2,39]
Co_3O_4	Exposed facets	[40]
$CoSe_2$	Redox potential	[41]
MoS_2	Defect-rich edges	[42]
CuS nanocluster	Oxygen vacancy concentration	[43]
Graphene quantum dots	Oxygen-containing functional groups	[19b,44]
Fe_3C-NC Nano balloons	Specific surface area, N and Fe contents	[45]

mechanistic and kinetic study will be reviewed, with the intension to deeply understand the structure–activity relationships and predictively design the activity prior to experiments.

3.1.2. Mechanistic and Kinetic Insights from Experiments

Kinetics: Experimental studies have shown that nanozyme catalysts, especially peroxidase nanozymes follow the Michaelis–Menten equation, which depicts the relationship between the reaction rate and the substrate concentrations.[47] The equation can be expressed as follows:

$$v_o = \frac{v_{max}[S']}{K_m + [S']} \quad (2)$$

where v_0 denotes the initial reaction rate, $[S']$ measures the initial substrate concentration, v_{max} represents the maximum reaction rate related to the catalytic rate constant k_{cat}, and K_m is the Michaelis constant, which is equal to the substrate concentration when $v_0 = v_{max}/2$.[48] Thus, K_m represents the affinity of the catalyst for the substrate, and lower K_m values correspond to higher interaction affinity between the nanozymes and the substrates.

Of note, the above Michaelis–Menten equation for nanozymes was obtained by fitting the experimentally measured apparent kinetics and drawing analogy with kinetic equation of natural enzymes. However, further analysis of the mechanism of the Michaelis–Menten kinetics is deserved, as some diffusion-process-controlled surface-reactions also show the similar kinetics.[49] As a result, the intrinsic materials features summarized in Table 1 cannot be integrated into this equation to offer it the prediction capability.

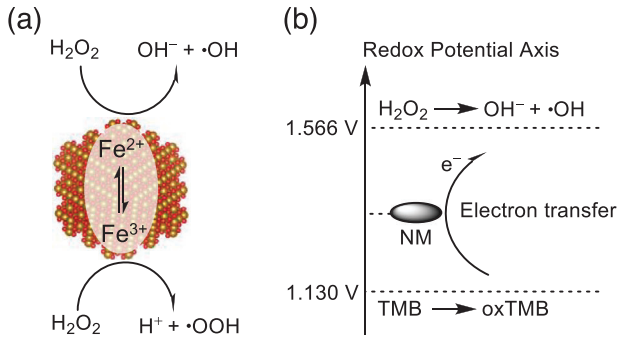

Figure 3. a,b) Mechanisms of peroxidase nanozymes from experiments: a) The free radical mechanism; b) the electron transfer mechanism. a) Reproduced with permission.[2] Copyright 2007, Springer Nature. b) Reproduced with permission.[50] Copyright 2014, American Chemical Society.

Free Radical Mechanism: Fenton-like reaction is the earliest mechanism proposed for the peroxidase-like activity of Fe_3O_4 nanoparticles. In 2007, Gao et al. showed that the catalytic activity of Fe_3O_4 nanoparticles behaving as peroxidase was pH, temperature, and H_2O_2 concentration dependent. The optimal pH and temperature were 3.5 and 40 °C, respectively.[2] Because •OH free radicals were detected by the electron spin resonance (ESR) technique in these studies, the Fenton-like mechanism was proposed to account for the catalytic activity of Fe_3O_4. The interconversion between Fe^{2+} and Fe^{3+} ions on the Fe_3O_4 surfaces, which resembles the Fenton catalysis with Fe^{2+} and Fe^{3+} ions, played the key role in the catalysis (**Figure 3**a).

Because it is analogous to the Fenton reaction, which has been well known since 1894,[51] the Fenton-like mechanism has been widely accepted to rationalize the peroxidase-like activities of many peroxidase nanozymes including Pt nanocrystals,[52] transition metal sulfide CuS and NiS,[53] Prussian blue (PB),[54] $MnFe_2O_4$@MOF,[55] and Cu_2MoS_4.[56] For example, Ma et al. found that cubic Pt nanocrystals could catalyze the oxidation of TMB through H_2O_2 to produce colored products to exhibit peroxidase-like activity.[52] They suggested that H_2O_2 molecule was split through a radical chain mechanism, in which electrons transferred from Pt to H_2O_2 to break the O–O bond to give •OH radicals. Continually, the resulting product •OH radicals were adsorbed on the Pt NPs surface to oxidize TMB to produce colored products (Figure 3a). The Fenton-like mechanism captures some of the features of the catalytic kinetics. It provides an easy way to understanding of the peroxidase-like activities of nanomaterials at the atomistic level.

Recently, Hang et al. found that the oxidation of TMB can be attributed to the generation of $O_2^{\bullet-}$ free radical via the peroxidase mimics catalytic activity of $MoSe_2$ nanostructures in the presence of H_2O_2, because the ESR signals of $O_2^{\bullet-}$ free radicals were detected in the experiment.[57] They proposed that the TMB molecules acted as chromogenic electron donors and were adsorbed on the $MoSe_2$ nanostructures. Then the electrons are transferred from TMB to $MoSe_2$, resulting in a significant increase in the electronic density and mobility on the surface of $MoSe_2$ nanomaterials, which facilitate the electron migration from $MoSe_2$ to H_2O_2 molecule. In the one-electron transfer process, large amounts of $O_2^{\bullet-}$ were generated, which oxidized TMB to yield the blue color.[57]

© 2023 Wiley-VCH GmbH

15214095, 0, Downloaded from https://onlinelibrary.wiley.com/doi/10.1002/adma.202211151 by Eth Zürich Eth-Bibliothek, Wiley Online Library on [11/07/2023]. See the Terms and Conditions (https://onlinelibrary.wiley.com/terms-and-conditions) on Wiley Online Library for rules of use; OA articles are governed by the applicable Creative Commons License

Electron Transfer Mechanism: Dong et al. comparatively studied the peroxidase-like activities of Co_3O_4 and Fe_3O_4.[50] Similar to Fe_3O_4, Co_3O_4 also showed considerable peroxidase-like activity.[50] Unlike the case of Fe_3O_4,[58] the ESR signal of •OH free radical was not detected in the case of Co_3O_4. To account for the peroxidase-like activity of Co_3O_4, the authors proposed the electron transfer mechanism (Figure 3b). According to this mechanism, the Co_3O_4 nanoparticles didn't interact with H_2O_2 via Fenton reaction. Alternatively, it acted as electron transfer mediators in the catalytic reaction. The Co^{3+} ions in Co_3O_4 first oxidized TMB by scratching an electron from TMB and the Co^{3+} was reduced to Co^{2+}. Then, the H_2O_2 was catalytically decomposed into OH^- by Co^{2+}. Meanwhile, the Co^{2+} was oxidized back to Co^{3+}. This mechanism was in line with the redox potential order: 1.566 V (H_2O_2) > 1.300 V (Co_3O_4) > 1.130 V (TMB). The redox potential of Co_3O_4 lied in between that of H_2O_2 and TMB, which made the electron transfer process feasible. The experiment showed that Co_3O_4 nanoparticle could oxidize TMB to produce the color change in the absence of H_2O_2 in acidic conditions, which verified the mechanism.

The authors reasoned that Fe_3O_4 nanoparticle followed the Fenton-like mechanism rather than the electron transfer mechanism because the redox potential of Fe_3O_4 was 0.711 V, which was not in between those of H_2O_2 and TMB.[50] Although electrons could be easily transferred from Fe_3O_4 to H_2O_2 molecules, but electrons are hard to be transferred from TMB to Fe_3O_4 to accomplish the catalytic cycle.[50]

The electron transfer mechanism and especially the redox potential model provided a quantitative understanding of the peroxidase-like activity of nanomaterials. This mechanism was also applied to understand the peroxidase-like mechanism of nanomaterials. Warkhade et al. found that $CoSe_2$ nanoflake (CS-nFs) exhibited an excellent peroxidase mimic activity.[41] The wide bandgap between H_2O_2 and TMB suppressed the direct electron transfer from TMB to H_2O_2. The reduction potential of CS-nFs (1.20 V) exactly lied in between that of H_2O_2 (1.566 V) and that of TMB (1.12 V), facilitating the electron transfer from TMB to H_2O_2 via CS-nFs (Figure 3b). The electron transfer mechanism was also applied to peroxidase nanozymes such as graphitic carbon nitride (g-C_3N_4).[59]

3.1.3. Mechanistic and Kinetic Insights from Computations

Mechanisms of Metals: Li et al. studied the mechanisms of the peroxidase-like catalyses of noble metal surfaces of Au, Ag, Pt, and Pd with periodic DFT calculations.[60] Following the idea of heterogeneous catalysis, they proposed that the H_2O_2 molecule first reacted with the metal surfaces to form the reactive oxygen-containing adsorbates. Then, the surface adsorbates reacted with TMB, through which the TMB was oxidized and the surfaces were recovered. Because noble metals were chemically inert, the authors hypothesized that the reductive removal of the adsorbates from the surfaces was facile and that the reaction of H_2O_2 with the metal surfaces was important. DFT calculations suggested that a H_2O_2 molecule had generally two reaction steps on the metal surfaces: The homolytic cleavage of H_2O_2 to form two OH* adsorbates, Equation (3), and the rearrangement of the two OH* adsorbates to form a H_2O* and an O* adsorbates, Equation (4). These two steps were written as follows:

$$H_2O_2{}^* = 2OH^* \quad (3)$$

$$2OH^* = H_2O^* + O^* \quad (4)$$

Hereafter, a surface reactive site is designated by asterisk and each surface adsorbate is labelled by an asterisk. The homolytic cleavage of H_2O_2 had the highest energy barrier and was the rate-determining step (**Figure 4**a). The authors calculated rate-determining energy barriers for the noble metals and found the energy barriers increased in the order: Au(111), Ag(111) > Pt(111) > Pd(111). This order was generally consistent with the experimentally observed increased peroxidase-like activity of these metal surfaces.[60]

To consider the influence of pH on the catalytic activity of noble metals, Li et al. assumed that protons and hydroxyl anions would adsorb on the metal surfaces, changing the reaction directions.[60] They further assumed that the adsorbed protons and hydroxyl anions transferred their charges away on the surfaces because of the good electron conductivities of metals. Therefore, they used the metal surfaces with the neutral hydrogen and hydroxyl adsorbates to model the metal surfaces in the acidic and basic conditions, respectively. However, because the hydrogen and hydroxyl adsorbates markedly changed the redox properties of the surfaces, the valid of this way of modelling the pH effect should be re-confirmed, especially material surfaces with poor electron conductivities. The redox potentials of H_2O_2 and $O_2{}^{\bullet-}$ are dependent on pH. Some of the pH-dependent enzyme-like activities could be understood by purely the thermodynamics of the catalytic reactions.[64]

Mechanisms of Nanoceria: Wang et al. comparatively studied the mechanisms of peroxidase-like activities of nanoceria with and without oxygen vacancies using periodic DFT calculations.[61] The catalytic mechanisms and energy profiles were shown in Figure 4b. First, H_2O_2 adsorbed at the surface of nanoceria. Second, the adsorbed H_2O_2 was decomposed into 2HO*. Third, the 2HO* were subsequently reduced by the two TMB-H^+ molecules. Protonated TMB (TMB-H^+) was used for this calculation, because TMB was considered to easily undergo the protonation reaction in the acidic conditions. Computational results showed that nanoceria with an oxygen vacancy located in the third layer of the surface (CeO_2-O_{3c}) possessed the highest peroxidase-like activity, which had a rate-determining energy barrier of 1.14 eV. However, on the surface of oxygen-vacancy-free nanoceria, the decomposition of H_2O_2 was unfavorable, in which the energy barrier was 2.15 eV. For CeO_2 with a subsurface oxygen vacancy (CeO_2-O_{2b}), H_2O_2 dissociated on the surface to form a H_2O molecule and an O atom, and O atom irreversibly filled the oxygen vacancy. The lower energy barrier of CeO_2-O_{3c} than that of oxygen vacancy-free accounted for the experiment finding that nanoceria with a higher oxygen vacancy concentration, namely, a larger fraction of Ce^{3+}, had a stronger peroxidase-like activity.[36a]

Mechanisms of sp^2-Carbon Systems: Hu et al. reported that the peroxidase-like activity of reduced graphene oxide (rGO) and mesoporous carbon could be enhanced by doping nitrogen heteroatoms.[62] To study the catalytic mechanism, DFT

© 2023 Wiley-VCH GmbH

15214095, 0, Downloaded from https://onlinelibrary.wiley.com/doi/10.1002/adma.202211151 by Eth Zürich Eth-Bibliothek, Wiley Online Library on [11/07/2023]. See the Terms and Conditions (https://onlinelibrary.wiley.com/terms-and-conditions) on Wiley Online Library for rules of use; OA articles are governed by the applicable Creative Commons License

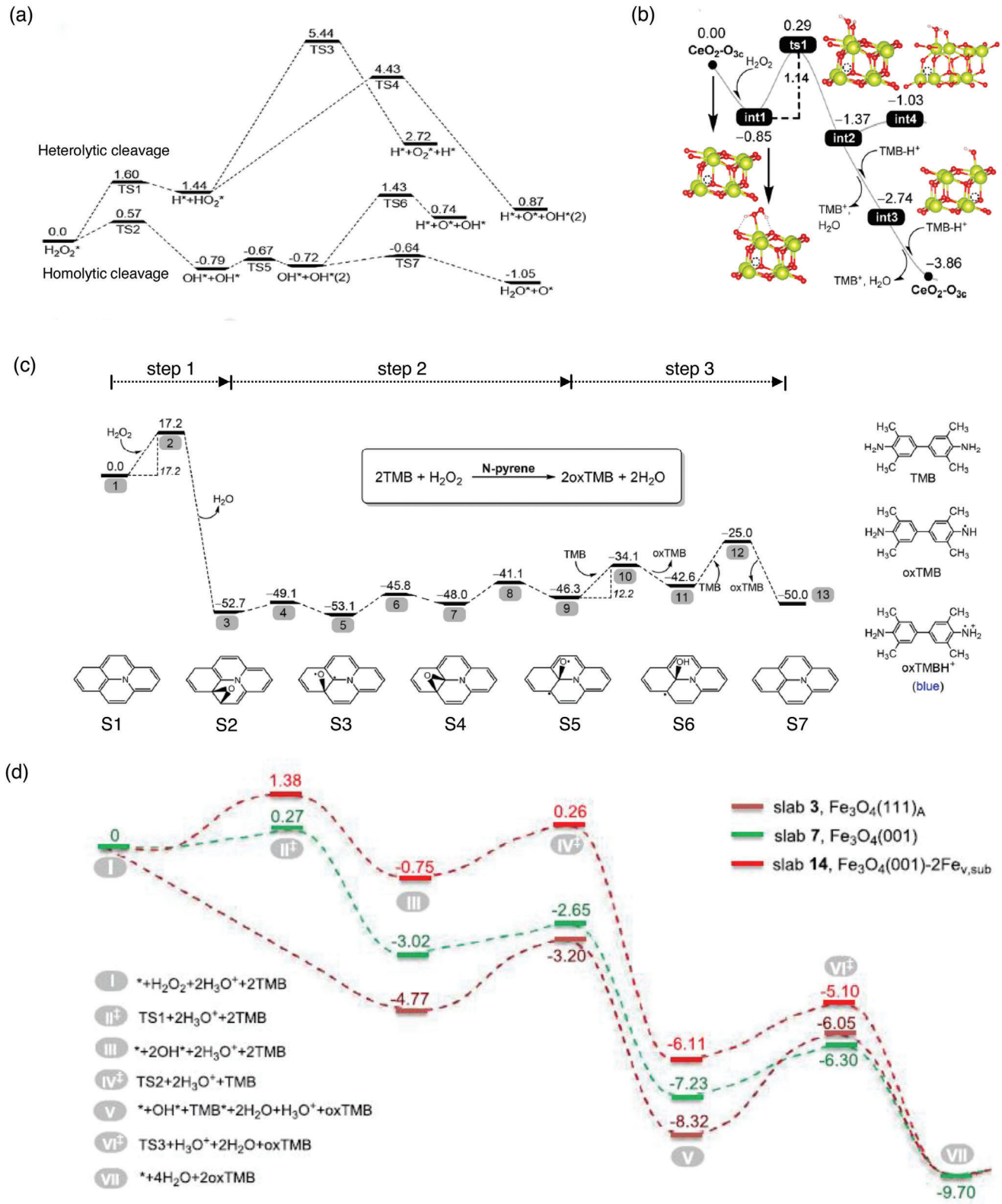

Figure 4. The mechanisms and kinetics of peroxidase nanozymes from DFT calculations. a) Au(111) (energy in eV). b) CeO_2 with oxygen vacancies (energy in eV). c) Nitrogen-doped graphene (energy in kcal mol^{-1}). d) Iron oxide slabs with different exposed facets and defects (energy in eV). a) Reproduced with permission.[60] Copyright 2015, Elsevier. b) Reproduced with permission.[61] Copyright 2021, American Chemical Society. c) Reproduced with permission.[62] Copyright 2018, American Chemical Society. d) Reproduced with permission.[63] Copyright 2020, American Chemical Society.

© 2023 Wiley-VCH GmbH

15214095, 0, Downloaded from https://onlinelibrary.wiley.com/doi/10.1002/adma.202211151 by Eth Zürich Eth-Bibliothek, Wiley Online Library on [11/07/2023]. See the Terms and Conditions (https://onlinelibrary.wiley.com/terms-and-conditions) on Wiley Online Library for rules of use; OA articles are governed by the applicable Creative Commons License

calculations using the cluster model (N-pyrene) were performed. The mechanism generally consisted of three steps (Figure 4c). First, the N-pyrene oxidized H_2O_2 to generate an epoxy intermediate (S2) and a H_2O molecule. Second, the epoxy O atom successively moved to the C atom adjacent to N (S5), and its conformation was changed from the epoxy to the axial bonding. Structure S5 was highly reactive owning to its unpaired electron. Third, the successive protonation of O atom by scratching two H atom from two TMB molecules. The third step for the O snatching the second H from the second TMB was the rate-determining step with an energy barrier of 17.6 kcal mol^{-1}. Importantly, the generated epoxy groups made strong covalent bonds with the carbon surface and were difficult to be reduced by TMB.[62] The enhanced activity by nitrogen doping could be ascribed to that the electron lone pair of the nitrogen atom improved the local electron density of the adjacent carbons.[65] Hu et al. further found that nitrogen doped rGO did not have catalase, oxidase, or SOD-like activity. The mechanism of the exclusive peroxidase-like of this material was also explained with their DFT calculation results.

The strategy of doping of heteratoms with electron lone pairs into the sp^2-carbon conjugated systems to enhance their catalytic activity was used in earlier studies on electrocatalyst such as oxygen reduction reaction,[66] photocatalytic.[67] Using a well-designed experiment, Sun et al. found that the carbonyl group in graphene oxide was the catalytically active site responsible for the catalysis and the carboxyl group was the binding site responsible for recruiting reactants.[19b] This mechanism was later supported by the DFT study of Gao et al.[68] The carbonyl groups actually introduced oxygen heteroatoms into the sp^2-conjugated system, in agreement with the above doping strategy. This doping strategy was later applied to achieve metal-free peroxidase nanozymes with high catalytic activities.[62,69]

Kinetic Equation: On the basis of the DFT mechanisms, Gao et al. derived a kinetic equation for the peroxidase-like nanozymes:[70]

$$v_0\left(H_2O_2\right) = ms\sigma \frac{A_1 e^{\frac{-\Delta G^{\neq}}{RT}}\left[H_2O_2\right]}{A_2 e^{\frac{\Delta G_1}{RT}} + \left[H_2O_2\right]} \quad (5)$$

where m is the mass of the nanozyme; s is the specific surface area; σ is average number of catalytically active sites per surface area; $\Delta G^{\neq}$ is the Gibbs free energy of activation of the rate-determining step; ΔG_1 is the change in Gibbs free energy relevant to the adsorption of H_2O_2 on the material surface; A_1 and A_2 are quantities whose formulation depends on the rate-determining step; $[H_2O_2]$ is the concentration of H_2O_2. Equation (5) has the same mathematical form as Equation (2), suggesting the underlying reason why the peroxidase-like nanozymes obey the Michaelis–Menten kinetic equation as the natural peroxidases. In Equation (5), m, s, and σ are the intrinsic global properties of the nanoparticles; $\Delta G^{\neq}$, ΔG_1, A_1, and A_2 are the intrinsic kinetic properties of the active center. Therefore, Equation (5) better bridges the enzyme-like catalytic activities with the intrinsic properties of nanoparticles than Equation (2). Equation (5) could be used to as the more powerful theoretical tool to study the structure–activity relationships of Table 1.

3.1.4. Descriptors and Prediction Models

Adsorption-Energy-Based Volcanic Plot: From a micro point of view, the catalytic activities of nanoparticles are determined by the total number of catalytically active sites and the activity of each site. Because the activity of the site is intrinsically governed by micro-kinetics and particularly the energy barriers, energy-based descriptors have been widely applied to predict catalytic activities of material surfaces.[71,72]

On the basis of the above heterogeneous catalytic mechanisms obtained by computations, Shen et al. developed a DFT-based method to predict the peroxidase-like catalytic activity of nanomaterials.[63] The authors investigated the mechanisms of peroxidase-like activity of iron oxide nanosurfaces using periodic DFT calculations. A total of 15 iron oxide nanosurfaces with different exposed facets, crystal structures, and chemical modifications were used as the iron oxide slab models.[63] The energy profiles of the full reaction pathways were investigated for seven slab models. Shown in Figure 4d are the profiles for Fe_3O_4(111), Fe_3O_4(001) and Fe_3O_4(001)-2$Fe_{v,sub}$. The result suggested that the catalytic mechanisms of different iron-oxide slabs were similar. The mechanism can be mainly divided into three steps. Step 1, the chemisorption of H_2O_2 onto the surface and the formation of two hydroxyl adsorbates. Steps 2 and 3, the consecutive reduction of the two hydroxyl adsorbates by the two TMB molecules to complete the catalytic cycle. This mechanism is also summarized in **Figure 5**a. However, the reaction kinetics of different iron-oxide surfaces were distinct: The rate-determining step varied from steps 1 or 3 for the different surfaces. For Fe_3O_4(001)-2$Fe_{v,sub}$ and Fe_3O_4(001), steps 1 and 3 had the highest energy barriers, corresponding to the rate-determining steps, respectively. Because reaction energy of step 1 ($E_{r,1}$), hydroxyl adsorption energy ($E_{ads,OH}$), and oxygen adsorption energy ($E_{ads,O}$) all approximately scaled linearly with the energies barriers of steps 1 and 3, these energies were the effective descriptors for predicting peroxidase-like activities of nanomaterials surfaces. Using $E_{ads,OH}$ as the activity descriptor, the volcano plot of peroxidase-like activity was obtained (Figure 5b). According to this volcano plot, a too weak adsorption affinity made step 1 hard to occur and be the rate-determining step, and a too strong adsorption affinity made step 3 hard to occur and be the rate-determining step. The energy window of activity is from −3.5 to −1.6 eV, and the surface site would have the optimal activity when $E_{ads,OH} = -2.6$ eV, neither not too strong nor too weak. The result that iron-oxide surfaces with moderate adsorption affinity had the best catalytic activity was consistent with the Sabatier principle for heterogeneous catalysis.[73]

According to the volcano plot, any feature influencing $E_{ads,OH}$ would influence the catalytic activity. Because atomic compositions, crystal structures, exposed facets, atomic vacancies, and chemical functionalization all change $E_{ads,OH}$ valued by changing the surface redox characters, such an $E_{ads,OH}$-based volcano plot could in principle explain the complex structure–activity relationship of Table 1, given that the precise atomic structures of the catalytic sites were known. For example, Figure 5b highlighted the role of surface Fe^{2+} sites in the catalysis. The surface containing more Fe^{2+} was more chemically reductive and thus had a stronger affinity for the OH group. Therefore, it provided a way to quantitatively understand the role of Fe^{2+} in the catalysis.

© 2023 Wiley-VCH GmbH

15214095, 0, Downloaded from https://onlinelibrary.wiley.com/doi/10.1002/adma.202211151 by Eth Zürich Eth-Bibliothek, Wiley Online Library on [11/07/2023]. See the Terms and Conditions (https://onlinelibrary.wiley.com/terms-and-conditions) on Wiley Online Library for rules of use; OA articles are governed by the applicable Creative Commons License

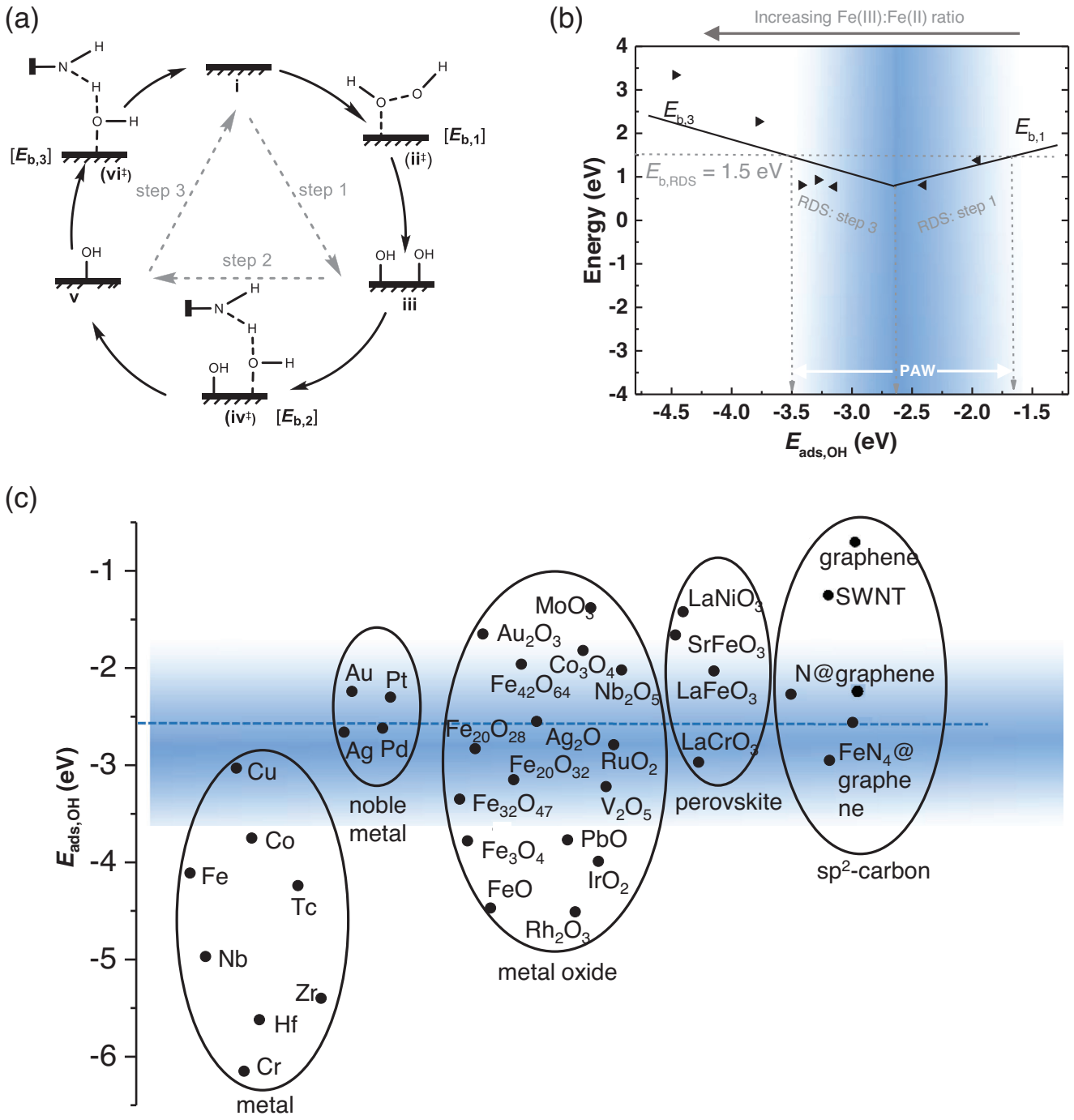

Figure 5. Mechanism and prediction model of peroxidase nanozymes. a) The three-step catalytic mechanism, in which E_{b1}, E_{b2}, and E_{b3} represent the energy barriers of three steps, respectively. b) Inverse volcano-shaped plot for the rate-determining step (RDS) energy barrier ($E_{b,RDS}$) with respect to the hydroxyl adsorption energy ($E_{ads,OH}$). c) Overview of the activity of peroxidase nanozymes. In (b) and (c), the blue zone is the peroxidase activity window (PAW) defined by the activity descriptor $E_{ads,OH}$; the color change from blue to white represents the gradual decrease of the activity. a–c) Reproduced with permission.[63] Copyright 2020, American Chemical Society.

The authors reasoned that the $E_{ads,OH}$-based volcano plot was also applicable to other peroxidase-like nanomaterials if they follow the catalytic mechanism of Figure 5a. On this basis, they calculated $E_{ads,OH}$ values for various materials surfaces, which included non-noble metals, noble metals, monometallic oxides, perovskites, and carbon nanomaterials, and plotted Figure 5c. The result of Figure 5c provided a bird's-eye view on the peroxidase-like activities of nanomaterials.

Redox Potential Model: On the basis of the electron transfer mechanism, Dong et al. proposed the redox potential model

© 2023 Wiley-VCH GmbH

15214095, 0, Downloaded from https://onlinelibrary.wiley.com/doi/10.1002/adma.202211151 by Eth Zürich Eth-Bibliothek, Wiley Online Library on [11/07/2023]. See the Terms and Conditions (https://onlinelibrary.wiley.com/terms-and-conditions) on Wiley Online Library for rules of use; OA articles are governed by the applicable Creative Commons License

to understand the peroxidase-like activities of Co_3O_4 and Fe_3O_4 nanoparticles (for details, see above discussion).[50] This model can be understood based on the reaction mechanism of Figure 5a. Regarding steps 2 and 3 of Figure 5a as one step, the three-step mechanism becomes the following two-step mechanism:

$$H_2O_2 + 2^* = 2OH^*,\ \Delta G_1 \quad (6)$$

$$OH^* + TMB + H^+ = H_2O + TMB^+ + {}^*,\ \Delta G_2 \quad (7)$$

where ΔG_1 and ΔG_2 are the Gibbs free energy changes of the corresponding reactions. For metal and metal oxide nanozymes, the reactants will form polar bonds with the materials surfaces and thus the mechanisms can be approximated as electron transfer processes without energy barriers. Then, ΔG_1 and ΔG_2, which determine the catalytic efficiency, can be approximately calculated with redox potentials of H_2O_2, nanomaterial, and TMB:$\Delta G_1 = -n\mathrm{F}[\varphi(H_2O_2) - \varphi(\mathrm{NM})]$;$\Delta G_2 = -n\mathrm{F}[\varphi(\mathrm{NM}) - \varphi(\mathrm{TMB})]$ (n denotes the charge number, F denotes the Faraday constant). Because $\Delta G_1 < 0$ and $\Delta G_2 < 0$ are the conditions for the reactions, the criterion $\varphi(H_2O_2) > \varphi(\mathrm{NM}) > \varphi(\mathrm{TMB})$, which is illustrated in Figure 3b, can be obtained. The redox potential model can provide a valuable estimation of the potential peroxidase activity of nanomaterials.

From a micro point of view, the redox potentials of nanomaterials correspond to the energy positions of the valence band maximums (VBMs) and conduction band minimums (CBMs) of the materials. Both VBMs and CBMs of nanomaterials may play the key role during the catalysis, depending on whether their energy positions are located in between the redox potentials of H_2O_2 and TMB. In case of Co_3O_4, the TMB first reduced the Co_3O_4 nanoparticle and the H_2O_2 oxidized the Co_3O_4 back to its original state.[50] Therefore, it can be inferred that the CBMs of Co_3O_4 played the key role. Because the fine electronic band structures can be determined using high resolution spectrometric techniques, the redox potential model may serve as the bridge between theory and experiment for nanozyme research.

Empirical Activity Descriptors: For some series of materials, the energy barriers of reactions occurring on them may depend on some particular features because the effects of other features are the same and cancelled. In this case, the features critically influencing the activity can also serve as the effective empirical activity descriptors. For example, the d-band center of metals[74] and the e_g occupation number of transition metal oxides[75] have been used as the activity descriptors for these materials in heterocatalysis. The effectiveness of these descriptors in enzyme-like catalysis were also observed.

Wang et al. showed that e_g occupation number was the effective descriptor of peroxidase-like activity of ABO_3-type perovskites, in which the A sites were alkaline-earth or rare earth metal and B sites were transition metals.[76] The e_g occupancies of B sites varied with the species of B (**Figure 6**a). The activity exhibited a volcano relationship with the e_g occupancy. As the e_g occupancy reached to ≈1.2 ($LaNiO_{3-\delta}$), the activity was the highest (Figure 6b). Shen et al. showed that the d-band center was the effective activity descriptor of the enzyme-like activities of noble metals.[77] The effectiveness of these descriptors can be ascribed to that these features critically influence the surface adsorption affinities and thus the overall catalytic energy barriers of the specific series of materials.

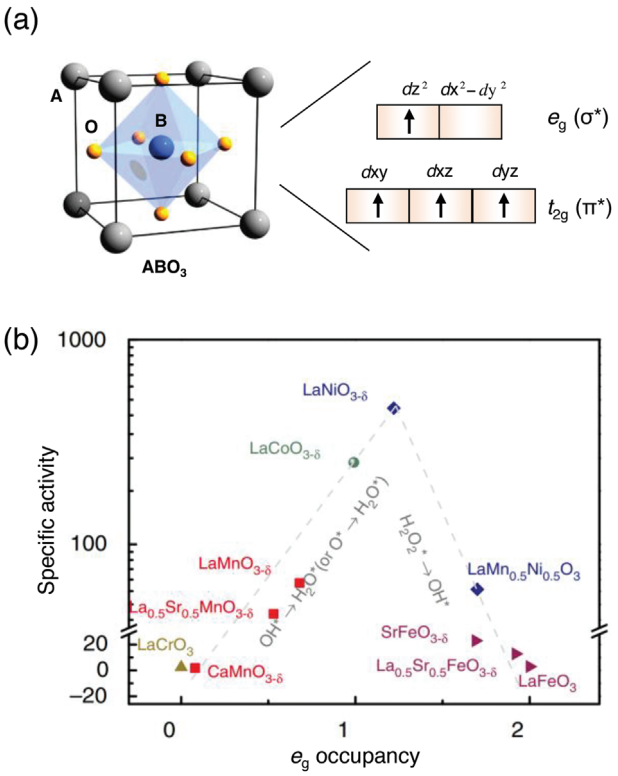

Figure 6. Describing the peroxidase-like activity of perovskites with the e_g occupancy number. a) Diagram showing the perovskite crystal structure and the metal d orbitals of the central metal, in which the e_g orbitals are marked. b) Volcano plot of the peroxidase-like activity with the e_g occupancy number for perovskites. a,b) Reproduced under the terms of the CC-BY Creative Commons Attribution 4.0 International license (https://creativecommons.org/licenses/by/4.0).[76] Copyright 2019, The Authors, published by Springer Nature.

3.1.5. Interplay between Experiments and Computations

The combined use of experimental and computational techniques is playing an increasingly important role in scientific research, which is also widely applied to the research and development of nanozymes in recent years. Xi et al. reported that the core–shell Ni–Pt nanoparticles, which consisted of nickel-rich cores and platinum-rich shells, exhibited the record-high peroxidase-like catalytic activity.[33d] DFT calculations were performed to understand the structure–activity relationship. The catalytic mechanisms suggested by the DFT calculations were shown in **Figure 7**a, which were generally consistent to those reported before (see above discussion).[33b,60,61] Adsorption-energy-based descriptors, $E_{ads,OH}$ and $E_{ads,O}$ were used to understand the dependence of the activity on materials compositions, which showed that the peroxidase-like activity increased with $E_{ads,OH}$ or $E_{ads,O}$. This result can be rationalized with the adsorption-energy-based volcano plot of Figure 5b. The alloying of nickel atoms into platinum nanoparticles greatly enhanced the d-bands of the metals, and thus increased the affinity of the surfaces for hydroxyl.

© 2023 Wiley-VCH GmbH

15214095, 0, Downloaded from https://onlinelibrary.wiley.com/doi/10.1002/adma.202211151 by Eth Zürich Eth-Bibliothek, Wiley Online Library on [11/07/2023]. See the Terms and Conditions (https://onlinelibrary.wiley.com/terms-and-conditions) on Wiley Online Library for rules of use; OA articles are governed by the applicable Creative Commons License

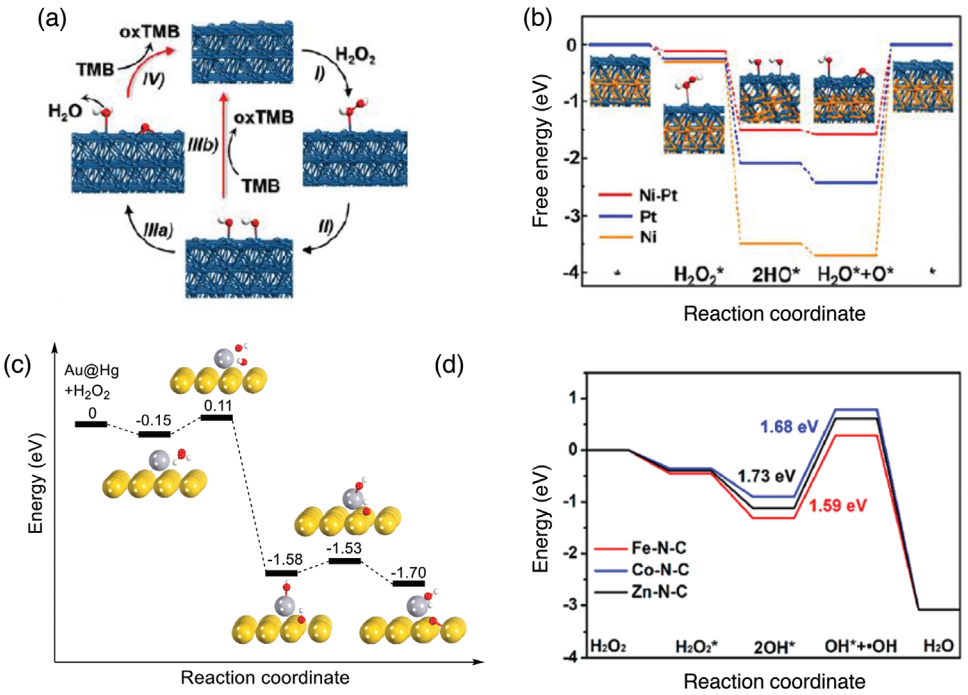

Figure 7. Mechanisms or reaction energy profiles for different peroxidase nanozymes. a) Pt nanoparticles; b) Ni–Pt, Pt, and Ni surfaces; c) The Au@Hg surface; d) M–N–C graphene-like materials (M = Fe, Co, and Zn). a,b) Reproduced with permission.[33d] Copyright 2021, American Chemical Society. c) Reproduced with permission.[78] Copyright 2021, Wiley-VCH. d) Reproduced with permission.[79] Copyright 2020, American Chemical Society.

Therefore, the rate-determining step became the reductive desorption of the oxygen adsorbate from the surface by TMB.[33d] Namely, the Ni–Pt nanoparticles are located in the left side of the volcano plot of Figure 5b, and therefore, an increasing $E_{ads,OH}$ resulted in an enhanced activity. The energy profiles of Ni–Pt, Pt, and Ni were shown in Figure 7b, which indeed suggested that the reaction of TMB with the oxygen adsorbate was the rate-determining step, in agreement with the prediction by the volcano plot of Figure 5b.

Chen et al. discovered that Hg atoms deposited on the Au film greatly accelerated the peroxidase-like activity of the Au film, and DFT calculation was performed to understand the mechanism.[78] The calculations suggested that the adsorption of H_2O_2 on Au(111)@Hg surface was more thermodynamically feasible than that on Au(111). The activation energy for H_2O_2 decomposition to 2OH* on Au(111)@Hg was only 0.26 eV (Figure 7c), which was lower than 0.6 eV for Au(111). The easier adsorption and activation of H_2O_2 on Au(111)@Hg than that on pure Au(111) and the experimentally observed higher peroxidase-like activity of the former than the latter suggested that these two species may located in the right side of the volcano plot of Figure 5b. Namely, the dissociative adsorption of H_2O_2 to the material surface was the rate-determining step. Of note, the energy barriers calculated for Au(111) and Au(111)@Hg using the PBE density functional may be severely underestimated.[80] The results obtained from calculations should be analyzed in conjugation with experimental results and the other knowledge.

Similar H_2O_2 adsorption followed by OH*/O* desorption mechanism and kinetics were widely reported for many other peroxidase nanozymes. Jiao et al. reported that densely isolated FeN_4 sites on M-N-C single-atom catalysts showed peroxidase-like activity superior to that on Zn(Co)-N-C nanozymes.[79] The higher reactivity was attributed to the strong adsorption energy of H_2O_2 and weak adsorption energy of two OH* on the FeN_4 site (Figure 7d). This means the adsorption of H_2O_2 and desorption of OH* were both facile, leading to its higher peroxides-like activity. A lot other examples can be also be found, which includes the studies of the peroxidase-like activities of Pt-single-atom modified carbon nitride,[81] FeN_3P single-atomic catalysts,[82] molybdenum-doped single-atoms,[46] palladium–iron-decorated graphydiyne nanosheets,[83] MoS_2 with sulfur defects,[42] and V_2O_5 nanowires.[38a,84]

3.2. Oxidase-Like Nanozymes

Nanomaterials can catalyze the oxidation of organic substrates such as TMB, glucose, ascorbic acid (AA), and 2,2'-azino-bis(3-ethylbenzothiazoline-6-sulfonic acid) (ABTS) by O_2 molecules, showing a chemical catalytic function similar to oxidases. Using TMB as the substrate, the reactions can be written as follows:

$$O_2 + 2TMB + 2H^+ = H_2O_2 + 2TMB^+ \quad (8)$$

$$O_2 + 4TMB + 4H^+ = 2H_2O + 4TMB^+ \quad (9)$$

The O_2 in the reaction of Equation (8) undergoes a two-electron reduction, being reduced to H_2O_2; in the reaction of Equation (9), the O_2 undergoes a four electron reduction, being reduced to H_2O. The four-electron reaction can also be regarded as the cascade of reaction Equation (8) and the peroxidase-like catalysis Equation (1).

© 2023 Wiley-VCH GmbH

15214095, 0, Downloaded from https://onlinelibrary.wiley.com/doi/10.1002/adma.202211151 by Eth Zürich Eth-Bibliothek, Wiley Online Library on [11/07/2023]. See the Terms and Conditions (https://onlinelibrary.wiley.com/terms-and-conditions) on Wiley Online Library for rules of use; OA articles are governed by the applicable Creative Commons License

15214095, 0, Downloaded from https://onlinelibrary.wiley.com/doi/10.1002/adma.202211151 by Eth Zürich Eth-Bibliothek, Wiley Online Library on [11/07/2023]. See the Terms and Conditions (https://onlinelibrary.wiley.com/terms-and-conditions) on Wiley Online Library for rules of use; OA articles are governed by the applicable Creative Commons License

3.2.1. Mechanistic Insights from Experiments

Perez et al. reported that dextran-coated nanoceria (DNC) could catalytic the oxidation of a series of organic substrates, such as TMB, ABTS, and DOPA, in the absence of H_2O_2.[85] The observed intrinsic oxidase-like activity for DNC was pH-dependent and exhibited optimally at acidic pH values. In addition, the oxidase-like activity was also dependent on the thickness of polymer coating and nanoparticles size. And a smaller size or thinner polymer coating nanoceira could behave a much higher catalytic activity.[85] Peng et al. found that the nanoceria could act as the oxidant instead of oxidase-like catalyst in the absence of oxygen, which was dissolved completely after being reduced by TMB.[86]

The ESR experiments have been widely applied to inspect the mechanism of oxidase-like activity of nanomaterials. Cheng et al. studied the molecular mechanism of the oxidase-like activity of nanoceria using hydroethidine as the $O_2^{\bullet-}$-specific fluorescence probe. They detected the signal of $O_2^{\bullet-}$ rather than that of HO• in the catalytic process. They proposed that O_2 could be reduced to $O_2^{\bullet-}$ at the defects site of nanoceria. Subsequently, the $O_2^{\bullet-}$ oxidized TMB via the electron transfer process.[87] Chen et al. found that the oxidase-like activity of Pr-modified ceria nanocubes was facilitated with the increase of the Pr amounts.[88] They proposed that the Pr incorporation introduced a Pr 4f band below the conduction band of Ce 4f, hence reducing the bandgap and assisting the electron transfer in the catalysis.[88] The proposed mechanism was also based on the observation of the $O_2^{\bullet-}$ signal in the catalytic process. Similar mechanism was also proposed for Mn_3O_4,[89] Fe-N-C single atom,[90] Pt-deposited multi-wall carbon nanotubes,[16b] carbon nanorod,[91] chondroitin sulfate modified platinum nanozyme (CS-PtNPs),[92] Mn-based single-atom enzyme (Mn/PSAE),[93] porous Co-Mn nanosheets with oxygen vacancies (OVs-CMO NSs),[94] and ZnCoFe triple-atom catalyst (ZNCoFe-TAC).[95]

3.2.2. Mechanistic Insights from Computations

Shen et al.[77] studied the mechanism for the four-electron oxidase-like activity of Au, Ag, Pd, and Pt using periodic DFT calculations. According to the mechanism, the $^3O_2$ molecule first accepted two electrons from metals to generate the peroxyl $(O_2)^{2-}$ adsorbate. Then, the O–O bond dissociated to form the isolated oxygen adatoms. These O-adatoms finally abstracted hydrogen atoms from organic substrates such as TMB to form the products (**Figure 8**a). Because of the chemical inertness of noble metals, the chemical desorption of O-adatoms by TMB was considered to be facile and the dissociative chemisorption of O_2 was considered the rate-determining step. Therefore, the energy barrier of the dissociation of O_2 could be used to theoretically estimate oxidase-like activity of this noble metal in catalyzing the oxidation of TMB. The energy barriers of the four metals increased with the order Pd < Pt < Ag < Au, which was generally consistent with the experimentally observed inverse activity order, supporting the reaction mechanisms and kinetics by computations. Because the O_2-dissociation energy barriers approximately scaled with the corresponding O_2 adsorption energies and the metal d-band centers, the latter two properties could be used to explain the oxidase-like activities of the four noble metals.[77] Similar O_2-adsorption initiated mechanism was proposed for the oxidase-like activity of nanoceria, which explained the role of oxygen vacancies in enhancing the activity of nanoceria (Figure 8b).[61] In this catalysis, the adsorbed O_2 might react with the $O_2^{\bullet-}$-probe molecules to yield the signal of $O_2^{\bullet-}$, in agreement with the experiment that $O_2^{\bullet-}$ signals could usually be detected for oxidase-like catalyses.[87,88]

Using the similar computational method, Cheng et al. studied the mechanism of the Au-catalyzed O_2-oxidation of glucose by periodic DFT calculations and suggested the mechanism different from the above O_2-adsorption initiated mechanism.[96] As shown in Figure 8c, glucose was first adsorbed on the Au surface, which would enhance the affinity of Au surface for O_2. Then, O_2 was adsorbed near the glucose adsorbate. The glucose successively transferred two H atoms to O_2 to form H_2O_2 with the assistance of Au surface, completing the catalytic cycle. The reaction process was thermodynamic and kinetic feasible (Figure 8d). The authors further studied the effect of phenylalanine (Phe) ligand of the Au surface in enhancing the selectivity of glucose oxidation. They comparatively studied the effects of deprotonated, neutral, and zwitterionic chiral Phe ligands on the Au surfaces. The results explained Phe-Au(111) showed high selectivity for the absorption of L-glucose and D-glucose. For the D-glucose, it preferred to absorbed on L-Phe-Au(111) and L-glucose prefer to D-Phe-Au(111) surface. The neutral and zwitterionic Phe ligand displayed greater selectivity. Finally, they conclude that chiral selective activity of Phe-Au come from the selective absorption of L(D)-glucose on covered surface.

3.2.3. Interplay between Experiments and Theory

One of the main properties experimentally observed for oxidase nanozymes is the substrate-dependent activity order. Zhang et al. found that the oxidase-like activity of Au@PdPt alloy could be tuned by the Pd/Pt ratio.[97] A lower Pd/Pt ratio could enhance the oxidation of AA and TMB; however, a higher Pd/Pt ratio was benefit for the catalytic oxidation of p-nitrophenol. Recently, Chen et al. revealed that the activity order was Au > Pt > Ru > Ir > Pd > Rh with glucose as the electron acceptor and that the order turned to Pt > Ir > Pd > Rh > Ru > Au with TMB as the electron acceptor.[98] The reduction product of O_2 varied from H_2O_2 and H_2O, which was dependent on the species of the catalysts. Jin et al. reported that the pH-dependent oxidase-like activity of sodium-modified iridium nanoparticles was mainly related to the substrate rather than the nanoparticles themselves.[33c] The microscopic mechanisms and kinetics have been studied to understand these structure–activity relationships.

The above mechanistic and kinetic results had been used to understand the experiment findings of oxidase nanozymes. Chen et al.[98] proposed a catalytic mechanism similar to the above glucose-adsorption-initiated mechanism for noble-metal catalyzed oxidation of glucose by O_2. Because the reaction occurred facilely under an alkaline condition, it was suggested that the OH^- could act as the Brønsted base and deprive hydrogen atoms from the hydroxyl group of glucose C1 site. In natural oxidases, the histidine residues function as such Brønsted

© 2023 Wiley-VCH GmbH

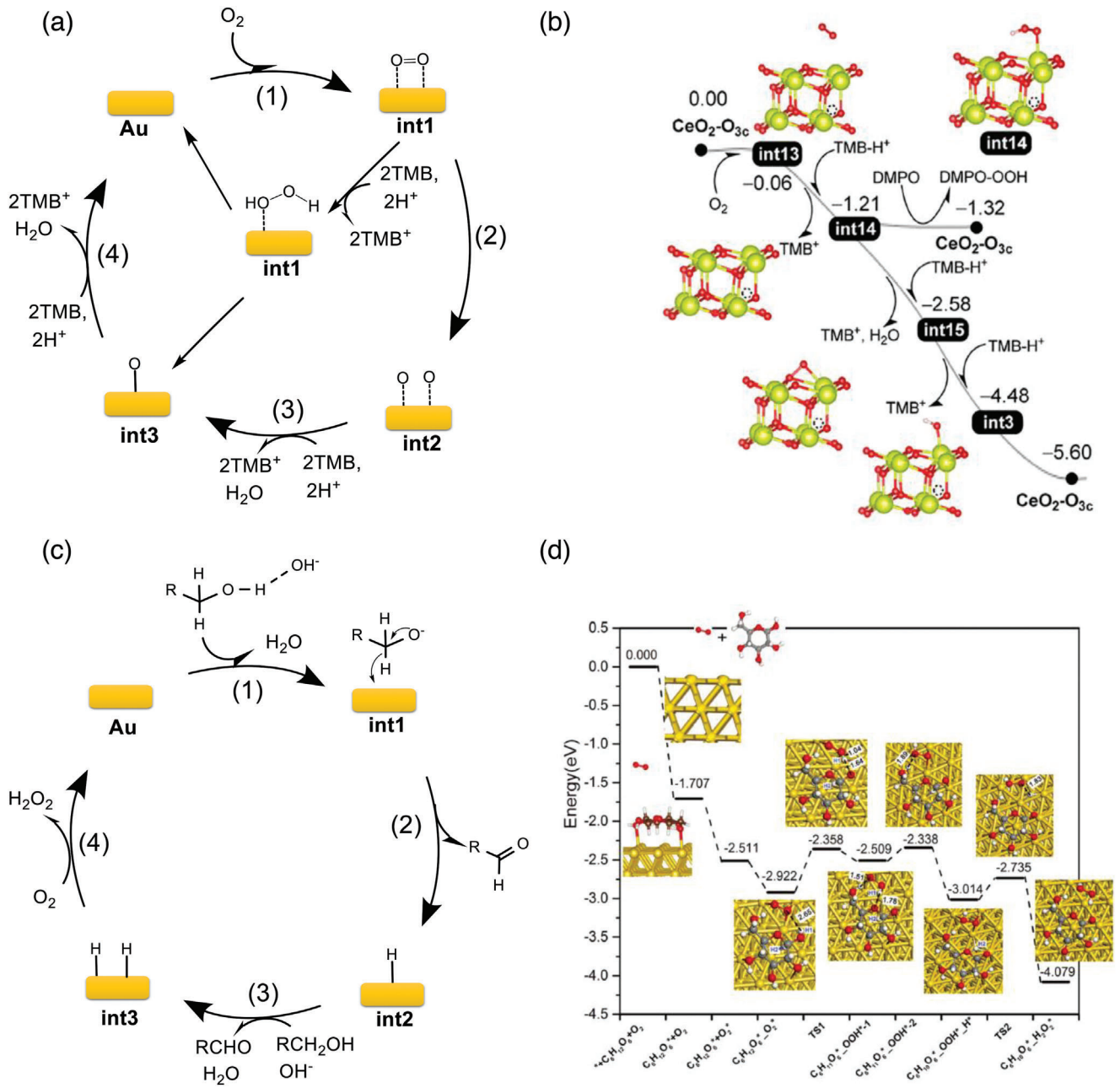

Figure 8. Mechanisms or reaction energy profiles for oxidase nanozymes by DFT calculations. a) Four-electron catalytic mechanism. b) Four-electron mechanism and the corresponding energy profile for CeO_2 with oxygen vacancy (energy in eV). c) Two-electron catalytic mechanism. d) Two-electron mechanism and the corresponding energy profile for the Au surface. a,b) Reproduced with permission.[61] Copyright 2021, American Chemical Society. c,d) Reproduced with permission.[96] Copyright 2020, Royal Society of Chemistry.

bases. The deprived hydrogen atoms were further transferred to noble metal surfaces, which produced the gluconolactone. The hydrogen atoms adsorbed on the metal surfaces reacted with O_2 to form H_2O_2 to complete the catalytic cycle (Figure 8c). For noble metals with peroxidase-like activity, the H_2O_2 was further catalytically reduced to H_2O by the glucose. The experimentally observed glucose oxidase-like activity order was Au > Pt > Ru > Ir > Pd > Rh. This suggests the initial glucose adsorption may play a key role in the catalysis, because this agrees with the fact that Au is the metal having the largest electronegativity and thus largest affinity for organic substrate, leading to its best catalytic activity. They further found that the activity order turned to Pt > Ir > Pd > Rh > Ru > Au in the case that TMB was the substrate. In this case, O_2-adsorption catalytic mechanism may be dominant, because this mechanism agrees with that Au has the smallest affinity for O_2 and thus the least catalytic activity. These results suggest that the mechanisms and kinetics of oxidase-like activity are dependent on the electron acceptors, and

© 2023 Wiley-VCH GmbH

15214095, 0, Downloaded from https://onlinelibrary.wiley.com/doi/10.1002/adma.202211151 by Eth Zürich Eth-Bibliothek, Wiley Online Library on [11/07/2023]. See the Terms and Conditions (https://onlinelibrary.wiley.com/terms-and-conditions) on Wiley Online Library for rules of use; OA articles are governed by the applicable Creative Commons License

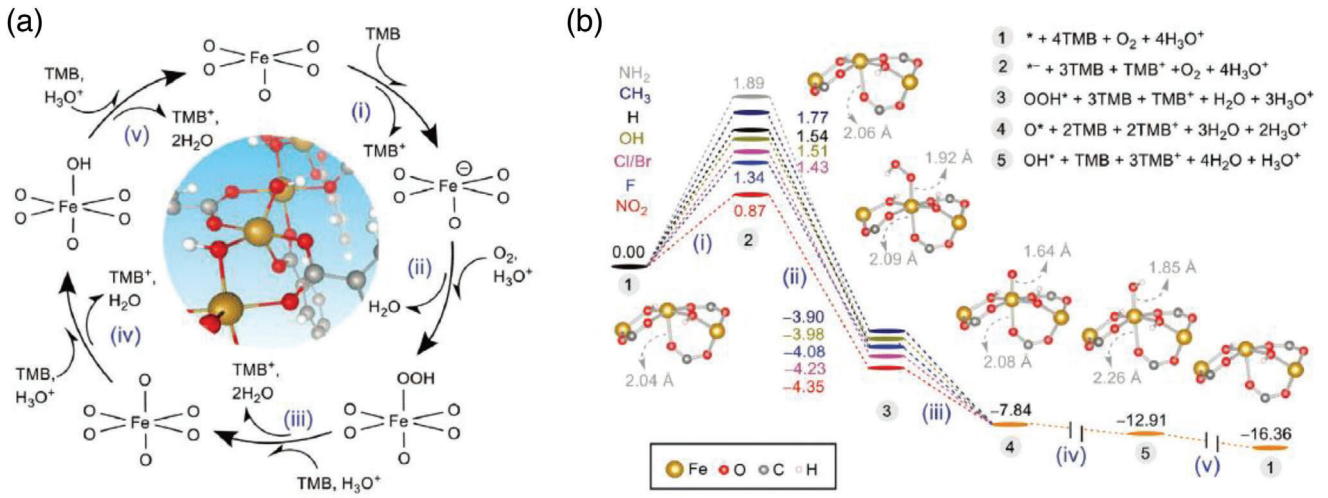

Figure 9. Mechanism and energy profile for the oxidase-like activity of the substituted metal–organic framework MIL-53(Fe)–X. a) Catalytic mechanism. b) Energy profile for the oxidation of TMB by MIL-53(Fe)–X. In (b), X = NH_2, CH_3, H, OH, F, Cl, Br, and NO_2, and the structures are for X = NO_2. a,b) Reproduced with permission.[99] Copyright 2020, Wiley-VCH.

atomistic level knowledge about the catalyst deserver further research efforts.

Wu et al. found that the oxidase-like activity of MOFs MIL-53(Fe)–X (X = NH_2, CH_3, H, OH, F, Cl, Br, and NO_2) in catalyzing the oxidation of TMB can be regulated by varying substituents attached to the MOFs organic linkers.[99] The activity scaled with the electron donating and withdrawing ability of the substituents. The strong electron-withdrawing substituent like NO_2 enhanced the activity and strong electron-donating substituent like NH_2 weakened the activity, as compared with that of the unsubstituted MOFs. The Hammett constants, which empirically describe the electronic substituent effects, could thus quantitatively predict the substituent-dependent activities of the substituted MOFs. The TMB-adsorption initiated mechanism was proposed with the aid of DFT calculations to interpret the structure–activity relationship (**Figure 9**a). The transfer of electron from the TMB to the MOF accompanying the initial TMB adsorption was assumed to be the rate-determining step (Figure 9b). Because an electron-withdrawing substituent lowered the energy position of conduction bands of MOFs and thus enhanced their oxidase-like activity by enhancing their ability to accommodating the electrons transferred from the TMB.

Ge et al. reported that cuboidal Pd(100) facet had better oxidase-like activity than the octahedral Pd(111) facet.[100] The O_2-adsorption initiated mechanism was proposed to interpret this facet-dependent activity. The dissociative chemisorptions of O_2 on the catalyst surfaces was considered to be the rate-determining step. DFT calculations suggested that the chemisorption of O_2 on the Pd(100) surface was more thermodynamic and kinetic feasible than that on the Pd(111) surface, which therefore explained the higher activity of the Pd(100) surface. Recently, Zhu et al. reported that the synergy effect between polyvinylpyrrolidone and oxygen vacancy could improve the oxidase-like activity of flower-like nanoceria.[101] The theoretical calculation indicated that oxygen vacancies could noteworthy enhance the adsorption affinity of nanoceria for O_2 and TMB, contributing to the enhancement of oxidase-like activity. Wang et al. investigated the mechanism and structure–activity relationship of oxidase-like activity of nanoceria, which also suggested that the presence of oxygen vacancy enhanced the activity.[61]

3.3. Superoxide Dismutase-Like Nanozymes

The SOD catalyzes the disproportionation of superoxide anion $O_2^{\bullet-}$. In this reaction, one $O_2^{\bullet-}$ anion transfers an electron to the other with the assistance of two protons, generating one H_2O_2 molecule and one O_2 molecule. The overall reaction can be written as follows:

$$2O_2^{\bullet-}+2H^+=H_2O_2+O_2 \quad (10)$$

Previous experiments have demonstrated that a lot of nanomaterials possess the activity in catalyzing the above reaction, being the SOD nanozymes. Following the experiments, the catalytic mechanisms the SOD-like activity of nanomaterials have been studied to understand the origin and guide the rational design of the activity.

3.3.1. Mechanistic Insights from Experiments

Ali et al. found that fullerene C_{60} derivative tris-malonyl (denoted as C_3 hereafter) was capable of eliminating $O_2^{\bullet-}$, possessing the SOD-like activity.[19a] The activity was highly related to the electron-deficient areas of the molecule, which were attractive for the $O_2^{\bullet-}$.[19a] Therefore, the activity was dipole moment-dependent, which was related to not only the number of carboxylic groups but their distribution on the surfaces of fullerene balls.[4b] Liu et al. showed that the SOD-like activity of water-soluble fullerenes was highly related with molecular properties including molecular structure, charge, and reduction potential.[102] More hydrogen bonds around the functionalized region of C_{60} cage, more positive charge, and higher redox potential imply higher SOD activities.

© 2023 Wiley-VCH GmbH

15214095, 0, Downloaded from https://onlinelibrary.wiley.com/doi/10.1002/adma.202211151 by Eth Zürich Eth-Bibliothek, Wiley Online Library on [11/07/2023]. See the Terms and Conditions (https://onlinelibrary.wiley.com/terms-and-conditions) on Wiley Online Library for rules of use; OA articles are governed by the applicable Creative Commons License

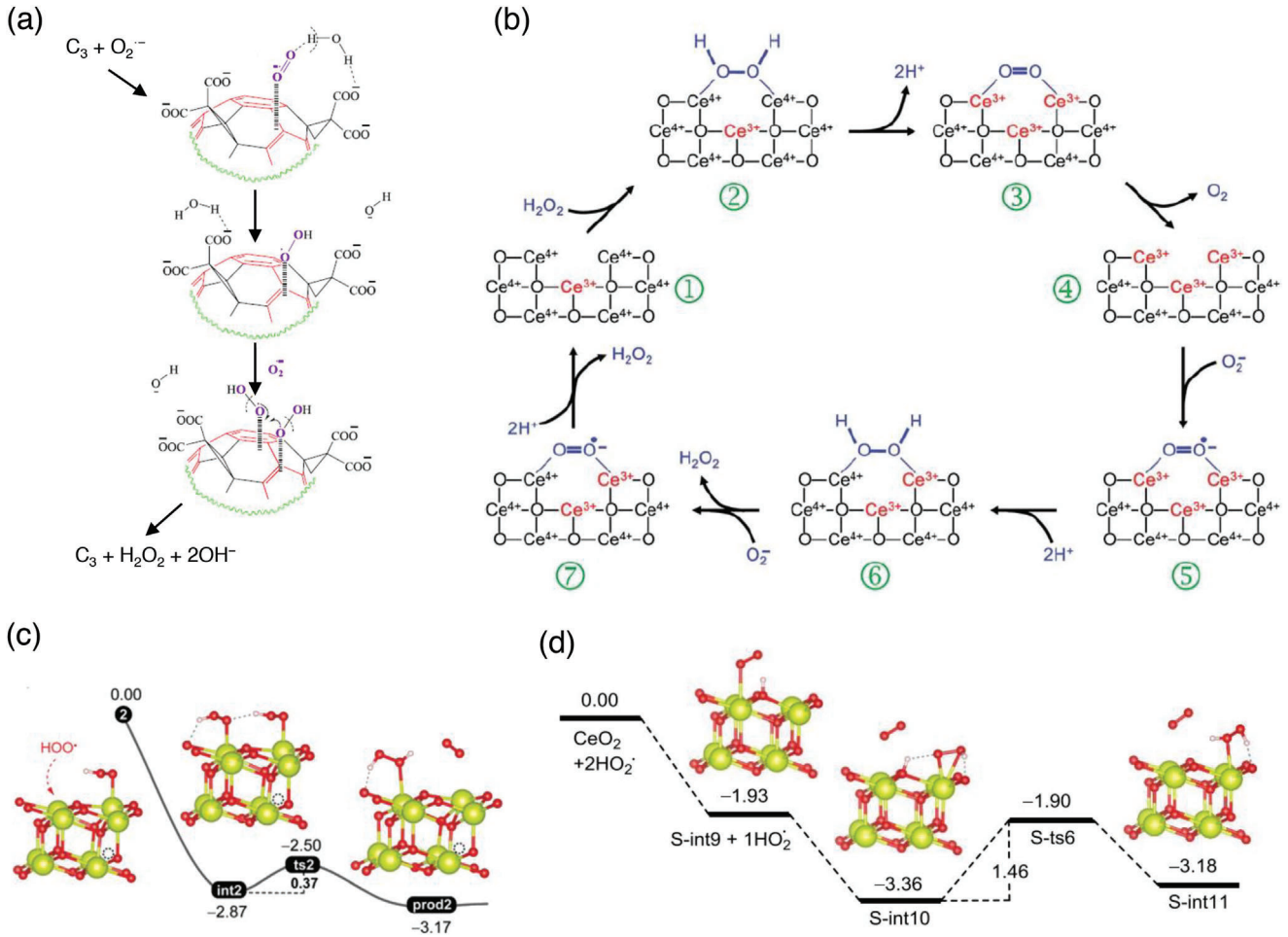

Figure 10. Mechanisms and reaction energy profiles for SOD nanozymes. a) The mechanisms proposed for the fullerene derivative C_3. Reproduced with permission.[19a] Copyright 2004, Elsevie. b) The mechanism proposed for CeO_2 with oxygen vacancies. Reproduced with permission.[104] Copyright 2011, Royal Society of Chemistry. c,d) The mechanisms and energy profiles for the rearrangement of two •OOH on CeO_2 with (c) and without (d) oxygen vacancy, respectively (energy in eV). c,d) Reproduced with permission.[105] Copyright 2019, Royal Society of Chemistry.

Dugan et al. proposed the following mechanism to explain the catalytic process: i) The $O_2^{\bullet-}$ first added to the electron-deficient segment and was stabilized by making hydrogen bonds with the carboxyl groups or the intercalated H_2O solvent; ii) the $O_2^{\bullet-}$ scratched protons from water or carboxyl groups to form the HOO* group on the carbon cage surface; iii) the above two steps were repeated for another $O_2^{\bullet-}$ to form another HOO*; iv) these two HOO* groups isomerized to form the O_2 and H_2O_2 molecules (**Figure 10**a).[19a] Because of the absence of a detectable paramagnetic intermediate in the experiments, a complete electron transfer between $O_2^{\bullet-}$ and C_3 was not considered in the proposed mechanism. The mechanism was also used to explain the SOD-like activity of fullerenol, another water-soluble fullerene derivative.[103]

Later, a similar mechanism was also proposed to understand the SOD-like activity of nanoceria. Korsvik et al. found that nanoceria possessed SOD-like activity and that the activity increased with the increase of the Ce^{3+}/Ce^{4+} ratio of the nanoceria.[4a] They speculated the possible mechanism for this catalysis: $O_2^{\bullet-}$ first reacted with the Ce^{4+} sites of nanoceria to produce O_2 and the Ce^{3+} sites. The reduced Ce^{3+} sites then further reacted with another $O_2^{\bullet-}$ in the presence of two protons to generate H_2O_2, through which the Ce^{3+} sites were changed back to Ce^{4+}. Following the idea of Ce^{4+} and Ce^{3+} interconversion, Celardo et al. also proposed a mechanism to account for the SOD-like activity of nanoceria with oxygen vacancies (Figure 10b).[104]

3.3.2. Mechanisms and Prediction Model from Computations

Osuna et al. studied the SOD-like mechanisms of C_3 using DFT calculations, in which the C_3 molecules were represented by the cluster models.[106] Wang et al. studied the mechanisms for the SOD-like activities of fullerenols using the similar computational method.[107] The mechanism suggested by calculations were generally consistent with the mechanism proposed by Dugan et al.[19a]

Wang et al. studied the mechanism of the SOD-like activity of nanoceria using periodic DFT calculations and the CeO_2(111) slab models.[105] To study the role of oxygen vacancies in the

© 2023 Wiley-VCH GmbH

15214095, 0, Downloaded from https://onlinelibrary.wiley.com/doi/10.1002/adma.202211151 by Eth Zürich Eth-Bibliothek, Wiley Online Library on [11/07/2023]. See the Terms and Conditions (https://onlinelibrary.wiley.com/terms-and-conditions) on Wiley Online Library for rules of use; OA articles are governed by the applicable Creative Commons License

catalysis, oxygen vacancies with different concentrations and locations were introduced into the slabs. The results indicated that the oxygen vacancies located in the subsurface and third-layer could assist the rearrangement of the two HOO* (i.e., protonated $O_2^{\bullet-}$) adsorbates on the material surface to form H_2O_2 and O_2, presenting the SOD-like catalytic activity. The nanoceria with the third-layer oxygen vacancy had the highest activity, with a moderate rate-determining energy barrier of 0.37 eV (Figure 10c). In contrast, oxygen vacancies located on the top surface would be irreversibly filled by the HOO* adsorbate, not showing the catalytic activity. The CeO_2 surface without any oxygen vacancy also did not show the catalytic activity, because both HOO* adsorbed on the surface were oxidized to O_2, and the formation of H_2O_2 encountered a higher energy barrier of 1.46 eV (Figure 10d). The results revealed the atomistic level mechanisms for the SOD-like activity and the role of oxygen vacancies in the catalysis. Because oxygen vacancies could migrate in nanoceria, the reveal reactions between $O_2^{\bullet-}$ and nanoceria would be more complex.

To develop a prediction model for SOD nanozymes, Wang et al. systematically considered the possible mechanisms of the SOD-like activity of nanomaterials and proposed the following two mechanisms:[64b]

Conduction band mechanism:

$$O_2^{\bullet-} + NM = O_2 + NM^-, \Delta G_3 \quad (11)$$

$$O_2^{\bullet-} + NM^- + 2H^+ = H_2O_2 + NM, \Delta G_4 \quad (12)$$

Valence band mechanism:

$$O_2^{\bullet-} + NM + 2H^+ = H_2O_2 + NM^+, \Delta G_5 \quad (13)$$

$$O_2^{\bullet-} + NM^+ = O_2 + NM, \Delta G_6 \quad (14)$$

In the above two mechanisms, the conduction band and valence band of nanomaterials played the vital role, respectively; ΔG_i (i = 3–6) were the corresponding changes of Gibbs free energy. Of the two mechanisms, the conduction band mechanism was similar to the mechanism previously proposed for the fullerene derivatives and nanoceria.[19a,105,107b] The condition for the conduction band mechanism to be thermodynamically spontaneous was $\Delta G_3 < 0$ and $\Delta G_4 < 0$. Because $\Delta G_3 = -nF[E_{CBM} - \varphi(O_2/O_2^{\bullet-})]$ and $\Delta G_4 = -nF[\varphi(O_2^{\bullet-},H^+/H_2O_2) - E_{CBM}]$, where CBM was the abbreviation of CBM, the condition could also be written as $\varphi(O_2/O_2^{\bullet-}) < E_{CBM} < \varphi(O_2,H^+/H_2O_2)$. This suggested the condition for the conduction band mediated SOD-like activity of nanomaterials. Likewise, the condition for the valence band mediated SOD-like activity of nanomaterials was $\varphi(O_2/O_2^{\bullet-}) < E_{VBM} < \varphi(O_2,H^+/H_2O_2)$, where VBM represented VBM. Because both VMB and CMB were the frontier molecular orbitals (FMOs) of the crystals, the thermodynamic condition of SOD-like activity was also summarized as: the nanomaterials should have at least one FMO whose energy was located in between $\varphi(O_2/O_2^{\bullet-})$ and $\varphi(O_2,H^+/H_2O_2)$. Because the electronic band structures of nanomaterials can be obtained with high resolution spectrum techniques and DFT calculations, the results paved the way to studying SOD nanozymes with the advanced experimental and computational methods.

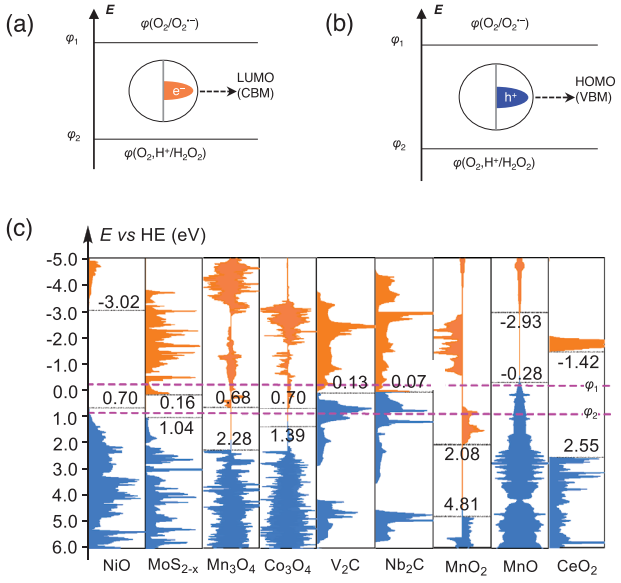

Figure 11. The prediction model of SOD nanozymes. a,b) Prediction models for the conduction-band-mediated (a) and valance-band-mediated (b) SOD-like activities of nanomaterials. c) The calculated electronic density of states for nine kinds of nanomaterials, in which the energies with respect to the energy of hydrogen electrode (HE) are marked. a–c) Reproduced under the terms of the CC-BY Creative Commons Attribution 4.0 International license (https://creativecommons.org/licenses/by/4.0).[64b] Copyright 2019, The Authors, published by Springer Nature.

The mechanisms were illustrated in **Figure 11**a,b, which provided a systematic understanding of the SOD-like activities of nanomaterials. Furthermore, the FMOs of several nanomaterials were calculated to support this mechanism (Figure 11c). It was suggested that nanomaterials such as NiO, MoS_{2-x}, Mn_3O_4, Co_3O_4, V_2C, and Nb_2C had FMOs (VBM or CBM) located in the energy level range [$\varphi(O_2/O_2^{\bullet-})$,$\varphi(O_2,H^+/H_2O_2)$], which affirmed that these nanomaterials possess SOD-like activity and were in consistent with precious experimental findings.[50,108] In addition, NiO was supposed to conduct a VBM-mediated mechanism. However, MoS_{2-x}, Mn_3O_4, Co_3O_4 were considered to conduct a CBM-mediated mechanism.

The energy level criteria of Figure 11 could be implemented to computationally screening nanomaterials with potential SOD-like activity. Besides the energy level criteria, Wang et al. further developed the adsorption energy criteria to predict the possible side reaction accompanying the SOD-like catalysis. On the basis both criteria, the authors screened 121 possible nanomaterials as potential SOD nanozymes from the 2D materials library[109] via high-throughput computation. The results shone light on the in-silico virtual screening of nanozymes from materials libraries.

3.4. Catalase-Like Nanozymes

Catalase is the enzyme catalyzing the disproportionation of H_2O_2. In this reaction, one H_2O_2 molecule transfers two hydrogen atoms to the other, generating one O_2 and two H_2O molecules. The overall reaction can be written as follows:

$$2H_2O_2 = 2H_2O + O_2 \quad (15)$$

© 2023 Wiley-VCH GmbH

15214095, 0, Downloaded from https://onlinelibrary.wiley.com/doi/10.1002/adma.202211151 by Eth Zürich Eth-Bibliothek, Wiley Online Library on [11/07/2023]. See the Terms and Conditions (https://onlinelibrary.wiley.com/terms-and-conditions) on Wiley Online Library for rules of use; OA articles are governed by the applicable Creative Commons License

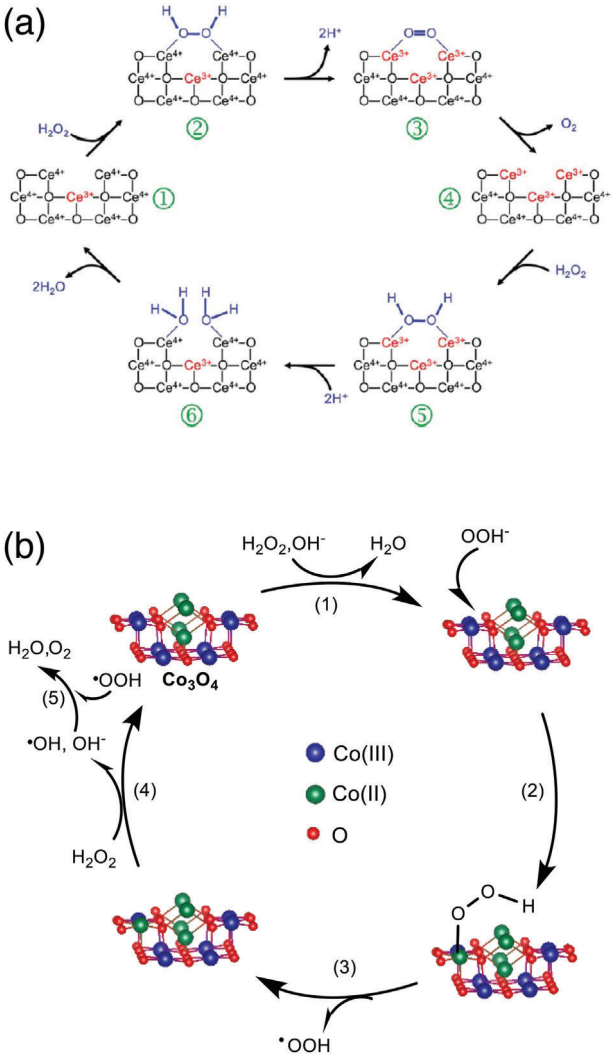

Figure 12. Mechanisms of catalase nanozymes from experiments. a) CeO_2 with oxygen vacancy. b) Co_3O_4 nanoparticles under alkaline condition. a) Reproduced with permission.[104] Copyright 2011, Royal Society of Chemistry. b) Reproduced with permission.[112a] Copyright 2013, Elsevier.

Many nanomaterials, such as nanoceria,[110] Fe_3O_4,[58] RuO_2,[111] and Co_3O_4,[112] were found to exhibit intrinsic catalase-like activity. The catalytic mechanisms had been studied.

3.4.1. Mechanistic Insights from Experiments

On the basis of the experiments that H_2O_2 could switch the oxidation state Ce atoms in nanoceria, Celardo et al. proposed the mechanism of **Figure 12**a to understand its catalase-like activity.[104] According to this mechanism, the H_2O_2 molecule first reacted with two Ce^{4+} sites of nanoceria to produce a molecular O_2 and two protons, reducing the two Ce^{4+} sites into Ce^{3+} (step i). Then, the second H_2O_2 molecule reacted with the two Ce^{3+} sites of nanoceria, through which the H_2O_2 was reduced into two H_2O molecules and the Ce^{3+} sites were oxidized back to Ce^{4+} (step ii). Sergio et al. also proposed a mechanism involving the interchange of Ce^{4+} and Ce^{3+} for the catalase-like activity of nanoceria.[110b] Similar mechanism was also proposed for the catalase-like activity of Co_3O_4 nanomaterials by Mu et al.[112b] What the different was that the OH^- in alkaline condition would facilitate the reaction proceeding of step i, which causing H_2O_2 to produce of O_2 and $2H_2O$ with the help of two OH^- first. At the same time, Co(III) was reduced to Co(II) by accepting two electrons from H_2O_2. Second, another H_2O_2 would accept two electrons from Co(II) and be reduced to $2OH^-$, and oxidize Co(II) back to Co(III). The reported catalase-like activity of Co_3O_4 was not only pH and temperature-dependent, but also morphology dependent. The catalytic activities followed the order of nanoplates > nanorods > nanocubes. The catalytic activity discrepancy was ascribed to their electron transfer diversities.[112b]

Wang et al. found that the catalase-like activity of Co_3O_4 was optimal in a condition with pH = 8.[112a] The five-step mechanism of Figure 12b was proposed to explain the reason why a high pH was in favor of catalysis. First, a H_2O_2 molecule reacted with a hydroxyl anion (OH^-) to give a perhydroxyl anion (OOH^-) and a H_2O molecule (step 1). Owing to its much higher nucleophilicity, the HOO^- group could interact with the metal sites of Co_3O_4 more easily than H_2O_2 to form •OOH radical (steps 2 and 3). Then, the Co_3O_4 nanoparticle catalyzed the homolytic cleavage of H_2O_2 through Fenton- or Haber–Weiss like reactions, generating the hydroxyl radical and hydroxyl anion (step 4). Finally, the •OOH radical formed in step II interacted with the hydroxyl radical formed in step III to generate the water and oxygen molecules, completing the catalytic reaction (step 5). The high pH enhanced the catalytic activity of Co_3O_4 by facilitating steps 1 and 2 of the reactions. The similar mechanism was also proposed to explain the catalase-like activities of Fe_3O_4.[58]

3.4.2. Mechanisms and Prediction Model from Computations

For a peroxidase-like catalysis, H_2O_2 serves as the electron acceptor and organic substrates like TMB serves as the electron donor (see Equation (1)). When H_2O_2 also served as the electron donor, the catalyzed reaction becomes H_2O_2 disproportionation (see Equation (15)). Namely, the catalase-like catalysis is intrinsically the specific kind of peroxidase-like catalysis. Indeed, Liu et al. found that the H_2O_2-adsorption-initiated three-step mechanism proposed for the peroxidase nanozymes also held for the catalase nanozymes.[113] The authors found that Pd nanoparticle supported on graphydine had good catalase-like activity, and the catalytic mechanisms was proposed by DFT calculations. First, the H_2O_2 molecule dissociatively adsorbed onto the catalyst to generate two OH* adsorbates (step i); then, the two OH* adsorbates were consecutively removed from the catalyst by the second H_2O_2 molecule as the hydrogen donor (steps ii). Step i had the highest energy barrier and was the rate-determining step. This suggests some peroxidase and catalase nanozymes have the same rate-determining steps, explaining the reason why the peroxidase and catalase-like activities of some nanomaterials have the same order. For example, the order Pd > Pt > Ag > Au have been found for both the peroxidase and catalase-like catalyses of the materials.[60,105,114]

Although many nanomaterials have stronger catalase-like activity in an alkaline condition, Zhang et al. found that the 2D

© 2023 Wiley-VCH GmbH

15214095, 0, Downloaded from https://onlinelibrary.wiley.com/doi/10.1002/adma.202211151 by Eth Zürich Eth-Bibliothek, Wiley Online Library on [11/07/2023]. See the Terms and Conditions (https://onlinelibrary.wiley.com/terms-and-conditions) on Wiley Online Library for rules of use; OA articles are governed by the applicable Creative Commons License

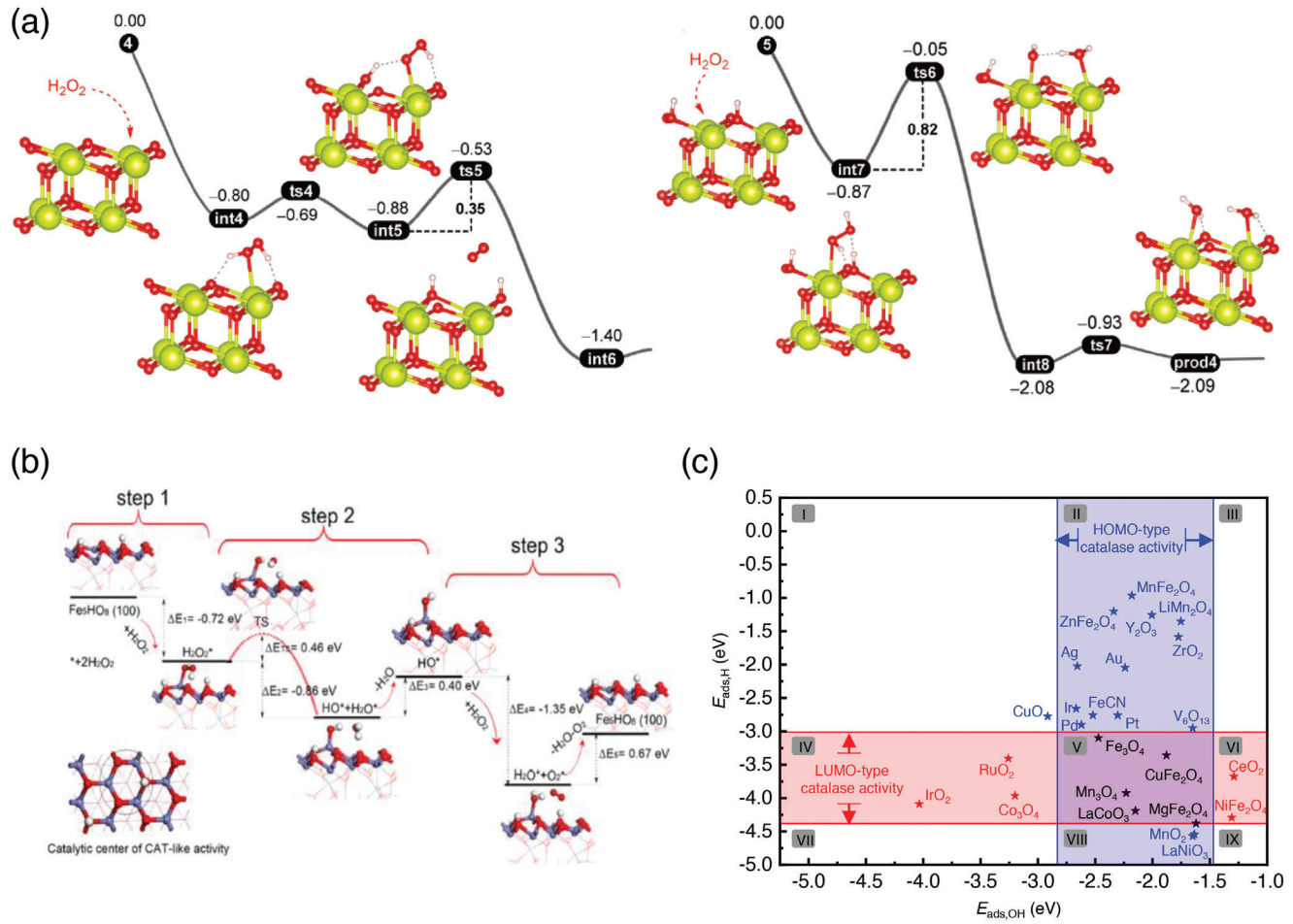

Figure 13. Mechanisms, reaction energy profiles, and prediction criteria of catalase nanozymes from DFT calculations (energy in eV). a) The CeO_2(111) facet. b) The ferrihydrite structure with H-terminated Fe_5HO_8(100) surface. c) Hydroxyl ($E_{ads,OH}$) and hydrogen ($E_{ads,H}$) adsorption-energy-based criteria of catalase-like activities of material surfaces. a) Reproduced with permission.[105] Copyright 2019, Royal Society of Chemistry. b) Reproduced with permission.[114] Copyright 2021, The Authors, published by Elsevier. c) Reproduced with permission.[70] Copyright 2022, Wiley-VCH.

nanomaterials MoS_2 exhibited better catalase-like activity under acidic conditions.[115] The authors performed DFT calculations to investigate the mechanisms. Four structural regions of the MoS_2 sheet, namely, the basic plane, S-edge, Mo–S-edge, and Mo-edge were considered as the potential active sites. The result suggested that only the S-edge was thermodynamically feasible to catalyze the disproportionation of H_2O_2. The mechanism was similar to the mechanism for the Pd and graphydine complex.

Li et al. studied the catalase-like activity of noble metals Au, Ag, Pt, and Pd using periodic DFT calculations.[60] Their calculations suggested that the H_2O_2 molecules always preferred to undergo the homolytic cleavage of the HO–OH bonds on the Au(111) surfaces, giving rise to water molecules and O* adsorbates. Because the recombination of O* adatoms to form O_2 molecules on the metal surfaces were not thermodynamically or kinetically favorable, they excluded the possibility that the catalase-like activity of noble metals was initiated by the HO–OH bond cleavage. Instead, they introduced a pre-adsorbed OH* on the metal surface to initiated the catalytic reaction and proposed the mechanism for the catalase-like activity of noble metal. They claimed that the pre-adsorbed OH* may represent the alkaline condition, in which the catalase-like activity of noble metal were maximal according to the experimental observations.[116] However, the introduction of a pre-adsorbed OH* adsorbate onto the catalyst surfaces to represent the alkaline condition was not well documented, the mechanism involving pre-adsorbed OH* may need further investigation.

Pirmohamed et al.[110a] observed that the catalase-like activity of nanoceria scaled positively with the Ce^{4+}:Ce^{3+} ratio of the materials, which was opposite to the case the SOD-like activity.[4a] Wang et al. studied the mechanism for the catalase-like catalysis of nanoceria using periodic DFT calculations.[117] Their results suggested a mechanism different from the above one. As shown in **Figure 13**a, the H_2O_2 molecule was first oxidized by the CeO_2 (111) surface, which gave rise to a molecular O_2 and two adsorbed H*. This step was different from the first step of the mechanism for the Pd and graphydine complex, in which the H_2O_2 was first reduced by the catalyst. Then, the two adsorbed H* reacted with another H_2O_2 molecule to yield two H_2O molecules and completed the catalytic cycle. The second step involved the breaking of the HO-OH bond and was the rate-determining step, which had an energy barrier of 0.82 eV. The introduction of an oxygen

© 2023 Wiley-VCH GmbH

15214095, 0, Downloaded from https://onlinelibrary.wiley.com/doi/10.1002/adma.202211151 by Eth Zürich Eth-Bibliothek, Wiley Online Library on [11/07/2023]. See the Terms and Conditions (https://onlinelibrary.wiley.com/terms-and-conditions) on Wiley Online Library for rules of use; OA articles are governed by the applicable Creative Commons License

vacancy into the nanoceria slab model made the first step thermodynamically less favorable, consistent with the experiment that nanoceria with a higher Ce^{4+}:Ce^{3+} ratio had a higher catalase-like activity.

Zhang et al. found that, unlike most nanomaterials that had both peroxidase-like and catalase-like catalytic activities, ferrihydrite had a specific catalase-like catalytic activity.[114] The exclusive catalase-like activity was related to the large numbers of hydroxyl groups contained on its surface, and the activity could be regulated by the surface hydroxyl abundance during the synthesis process. DFT calculations showed that during a complete catalase-like catalytic cycle, the H atoms of hydroxyl groups on the material surface could promote the cleavage of the HO–OH bond of the first H_2O_2 molecule to produce H_2O and H vacancy. While the second H_2O_2 molecule was located closely to the catalytic centers, the hydrogen vacancy can more easily capture the hydrogen atom from H_2O_2, thereby prompting it to break the oxygen-hydrogen bond to generate O_2 and another H_2O without energy barriers (Figure 13b).

To develop a prediction model for catalase nanozymes, Gao et al. systematically considered the possible mechanisms of the catalase-like activity of nanomaterials and proposed the following two mechanisms:[70]

Valence band mechanism:

$$H_2O_2 + 2^* = 2OH^* \quad (16)$$

$$2OH^* + H_2O_2 = O_2 + 2H_2O + 2^* \quad (17)$$

Conduction band mechanism:

$$H_2O_2 + 2^* = 2H^* + O_2 \quad (18)$$

$$2H^* + H_2O_2 = 2H_2O + 2^* \quad (19)$$

The authors further suggested that hydroxyl ($E_{ads,OH}$) and hydrogen ($E_{ads,H}$) adsorption energies to the activity descriptors of the valence- and conduction-band-mediated catalase-like activities, respectively. The material surfaces are predicted to have the valence-band-type activity when -2.83 eV $< E_{ads,OH} < -1.47$ eV and the conduction-band-type activity when -4.38 eV $< E_{ads,H} < -3.01$ eV.[70] Using these criteria, the mechanisms of the catalase-like activities of the nanomaterials have been systematically understood using Figure 13c. Because these criteria are purely based on thermodynamics of the reactions, they should be applicable to nanozymes derived from metals and metal oxides. Instead, they should be inapplicable to covalent-material-based nanozymes, on which the OH and H adsorbates make strong chemical bonds with the material surfaces and the energy barriers of the reactions are important.

4. Other Nanozymes

Except for the above oxidordeuctase enzymes, which catalyze the degradation of O_2, H_2O_2, and $O_2^{\bullet-}$, nanomaterials mimicking the activities of other enzymes have been also reported.

4.1. Dehydrogenase-Like Nanozymes

Dehydrogenase is a class of enzyme that catalyzes the dehydrogenation of organic substrates. Gu et al. reported that black phosphorus nanosheets could mimic glucose dehydrogenase activity to oxidize the oxidation of glucose without the byproduct H_2O_2, which was different from glucose oxidase.[118] Zhang et al. reported that gold nanoparticles could mimic dehydrogenase to convert estradiol to estrone.[11] Gao et al. found that 2D SnSe nanosheets was capable of mimicking lactic dehydrogenase to effectively catalyze the hydrogen transfer.[119] Their DFT calculations suggested that SnSe nanosheets with Sn vacancy detached hydrogen from lactic acid with the lowest reaction energy (4.4 kcal mol^{-1}), showing the best catalytic activity. The proposed catalytic mechanism suggested that the hydrogen adsorption energy might be the descriptor of the catalytic activity. However, further DFT studies are needed for an in-depth understanding of on the catalytic mechanisms and kinetics dehydrogenase nanozymes.

4.2. Hydrolase-Like Nanoymes

Hydrolase is a family of enzymes that catalyze the hydrolysis of chemical bond of multifarious substrates, such as phosphate esters, carbohydrates, and amides. Although the catalytic mechanisms varied with the substrate structures, the overall reactions are similar. Vernekar et al. found that vacancy-engineered nanoceria could act as phosphotriesterase to catalyze the degradation of nerve agents.[120] It was supposed that Ce^{III} provided adsorption site for water, and subsurface Ce^{IV} was the adsorption site for paraoxon. The adjacent adsorption allowed the nucleophilic attack of water or hydroxide to the phosphorus centers, facilitating the hydrolysis of phosphoester bond. In addition, MOFs consisting of Ce^{IV} and Zr^{IV}, such as NU-1000,[121] MOF-808,[122] UiO-66,[123] Ce-based MOF[124] etc., were found to possess high phosphohydrolase performance. The activities were commonly attributed to the M–OH–M two-metal-ion structures, in which the metal-active sites acted as the Lewis acids and the OH^- nucleophilic attacked the electrophilic P-site, causing the decomposition of substrates. Moon et al. found the available coordination number of the active metal site could affect the catalytic activity.[125] The activity of Zr-based MOFs decreased with the available linker number and followed the order MOF-808 (6-free) > NU-1000 (4-free) > UiO-66 (0-free). However, DFT calculations by Momeni et al. suggested that more available coordination number could also increase the activation energy and lower the catalytic activity.[126] In addition, the substitution of Zr^{IV} with Ce^{IV} could also reduce the activation energies to enhance the activity of UiO-66-10-I and MOF-808. Recently, on the basis of the catalytic mechanisms and kinetics revealed by DFT calculations, Li et al. developed the co-adsorption energy model to predict the activities of material surfaces in mimicking the phosphohydrolases. Guided by the prediction model, the phosphohydrolase-like nanozyme based on noble metal Ru was experimentally found.[29b]

© 2023 Wiley-VCH GmbH

15214095, 0, Downloaded from https://onlinelibrary.wiley.com/doi/10.1002/adma.202211151 by Eth Zürich Eth-Bibliothek, Wiley Online Library on [11/07/2023]. See the Terms and Conditions (https://onlinelibrary.wiley.com/terms-and-conditions) on Wiley Online Library for rules of use; OA articles are governed by the applicable Creative Commons License

5. Non-Catalytic Self-Depleting Reactions

Catalyst can speed up the reaction rates without changing their chemical compositions and masses before and after the reactions. However, practical catalysts usually have irreversible side reactions that deplete the active centers of the catalysts. Wang et al. computationally studied the mechanisms of the peroxidase, oxidase, catalase, and SOD-like activities of nanoceria with oxygen vacancies by DFT calculations.[61,105] Aside from the catalytic cycles, side reactions in which the oxygen-containing reactants irreversibly filled the oxygen vacancies and changed the Ce^{3+} to Ce^{4+} were also found. Therefore, the oxygen vacancies and the associated Ce^{3+} sites, which served as the active centers of the enzyme-like catalyses, were continuously consumed during the catalyses. Recently, Dong et al. experimentally demonstrated that the peroxidase-like activity of Fe_3O_4 could indeed be depleted by the side reactions, which oxided Fe_3O_4 into γ-Fe_2O_3 during the catalysis.[127] These results suggested the importance of designing and synthesizing stable nanozymes with long service lifetimes.

6. Machine-Learning Prediction Models

In contrast to the mechanisms and kinetics-based prediction models,[44,60,77,105] The machine-learning algorithms are particularly useful to develop the quantitative structure–activity relationships for systems when the underlying mechanisms of the relationships are unknown or too complicated to disclose.[128] A number of the data-informed machine-learning models predicting the enzyme-like activities of nanomaterials have also been established recently. Wei and co-workers used the data-informed strategy to design new hydrolase nanozymes.[129] Wei et al. developed fully connected deep neutral network (DNN)-based models to classify and quantify the enzyme mimetic activities of nanomaterials via machine learning.[130] Razlivina et al. developed a random forest regression model to evaluate the activity of peroxidase nanozymes.[131] Zhang et al. established the machine-learning models to select candidates of SOD nanozymes.[132] Yu et al. achieved the machine-learning model that efficiently calculated the energy barriers for the peroxide-like catalyses of heteroatom doped graphydiyne.[133] Gao et al. developed the explainable and efficient machine-learning models for the virtual screening of 2D nanozymes to target tumor hydrogen peroxide.[70] These results suggest that the data-based machine-learning methods have great potentials in the in silico design of nanozymes on the condition that the underlying mechanisms and kinetics of the catalyses are too complicated to disclose by the DFT method.

7. Concluding Remarks and Future Perspectives

The recent progress in the study of the microscopic mechanisms and kinetics of nanozymes has been reviewed. Nanozymes usually refer to inorganic nanomaterials with enzyme-like catalytic activities. They are superior to natural enzymes in several aspects and are promising to replace natural enzymes in a variety of applications. The microscopic mechanisms and kinetics of nanozymes, which underlie the experimentally observed catalytic activities, are among core knowledge for the in-depth understanding and predictive design of nanozyme activities. However, the corresponding study is not easy because most nanozymes are amorphous nanomaterials and catalyses occur in complex water environments. DFT calculations, which can provide atomistic-level insights into the reaction mechanisms and kinetics, have been playing an increasingly important role in the research and development of nanozymes in the recent years. The computational studies have to some extent bridged the gap between the macroscopically observed activities and the microscopic structures and compositions of nanozymes.

The essence of nanozyme catalyses is the heterogeneous chemical reactions occurring on nanomaterials surfaces. Because DFT calculations can give a comprehensive prediction of the geometries and energies of species involved in the reactions, the microscopic mechanisms obtained by DFT can serve as the general basis of other mechanisms that have ever been proposed to understand the catalytic activities of the specific nanozymes. Likewise, the activity descriptors and prediction models based on the micro-mechanisms and kinetics by DFT can also serve as the basis of other empirical prediction models. The relationships of the different mechanisms and models of peroxidase nanozymes are shown in **Figure 14** as the example. The following concluding remarks can be summarized for the relationships. 1) The free radical mechanisms proposed for nanozymes cannot be evidenced by the observation of the free radical signals using, for example, the ESR technique. These techniques do not necessarily demonstrate the generation of the free radicals in the solid–liquid catalytic systems, like nanozymes, because the free radical probe molecules can also react with the surface adsorbates to generate the signals. Therefore, the free radical mechanisms proposed for nanozymes may need to be revisited. The observation of the signals only reflects that the free radical-like adsorbates have ever been formed on the nanozyme surfaces as the reaction intermediates, which instead support the DFT mechanisms.

2) The Fenton-like mechanism for peroxidase nanozymes is proposed based on the observation of the •OH signals using the free radical trapping agents. Likewise, the signals may be produced by the direct reaction between the trapping agents and the OH* adsorbates on the nanozyme surfaces, which does not necessarily signifies the formation of the free radicals. Furthermore, •OH radicals have very poor selectivity when reacting with organic substrates because of their ultrahigh reactivity, which is inconsistent with the considerable substrate selectivity that have been demonstrated for peroxidase nanozymes. Because it does not properly reflect the mechanistic and kinetic features of the reactions, the Fenton-like mechanism is not recommended for peroxidase nanozymes.

3) The electron-transfer mechanisms and the corresponding redox potential models are valid on the condition that the catalytic reactions of nanozymes are net electron transfer processes and that the reactions are thermodynamics controlled with low energy barriers. This approximation normally oversimplifies the reactions occurring on nanozymes, especially nanozymes based on covalent materials like graphene and the derivative, for which the rearrangements of molecular orbitals and the contribution of energy barriers to the reaction kinetics are also important. However, because this mechanism and prediction model to some extent reflects the reaction energies of the nanozyme catalyses, they provide simple but useful theoretical tools for understanding the activities of nanozymes.

© 2023 Wiley-VCH GmbH

15214095, 0, Downloaded from https://onlinelibrary.wiley.com/doi/10.1002/adma.202211151 by Eth Zürich Eth-Bibliothek, Wiley Online Library on [11/07/2023]. See the Terms and Conditions (https://onlinelibrary.wiley.com/terms-and-conditions) on Wiley Online Library for rules of use; OA articles are governed by the applicable Creative Commons License

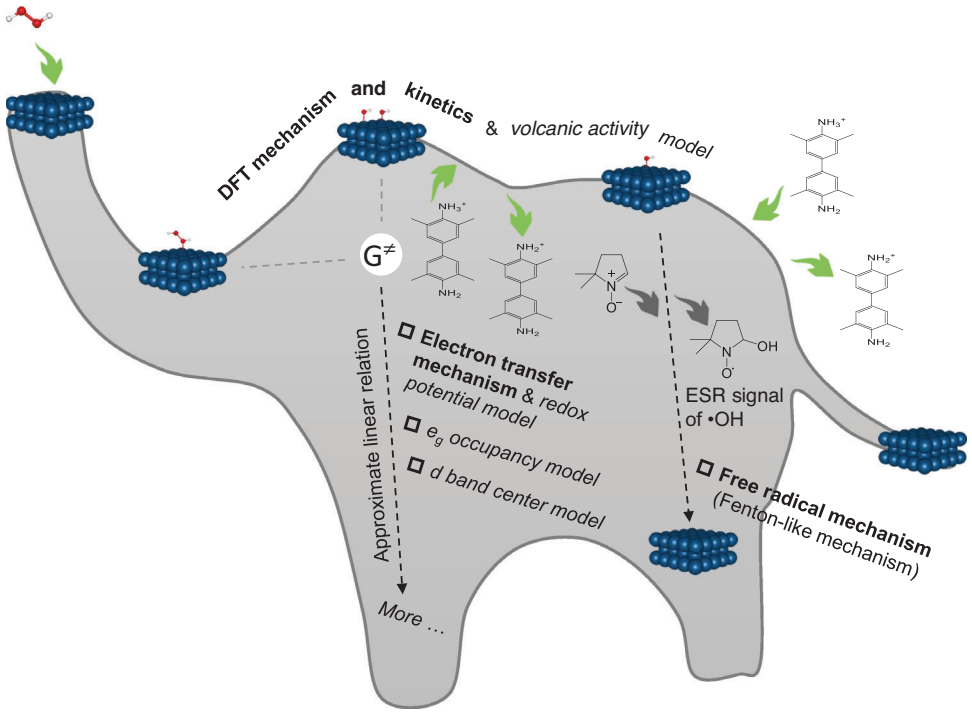

Figure 14. The relationship of different mechanisms and prediction models of peroxidase nanozymes. The DFT mechanism can be the basis of other mechanisms and the volcanic activity model can be the basis of other empirical prediction models.

4) The DFT mechanisms and kinetics are based on the potential energy surfaces of the catalytic reactions of nanozymes, which are explicit in physics and rigorous in physicochemical principles. Therefore, they are possible to closely interplay with the advanced experimental approaches that are built on the same physicochemical foundations. The DFT mechanisms and kinetics for peroxidase, SOD, catalase, and oxidase nanozymes have been extensively studied, and the prediction models for peroxidase and SOD nanozymes have also been established. However, DFT calculations normally treat reaction systems with no more than hundreds of atoms. Their applications to real nanozymes usually encounter severe limitations, e.g., the inhomogeneous compositions and exposed facets, unclear structures of active sites, and unknown side reactions of the nanozymes. The power of DFT calculations can only be maximized in combination with the elaborately-designed experiments.

Undoubtedly, the combination of DFT calculations and experiments will still be the most powerful way for the research of the catalytic mechanisms and kinetics of nanozymes in the future. To better promote the research, establishing a nanozyme library with well-characterized structures and enzyme-like activities will be highly desirable, which will serve as the starting points and benchmarks of the DFT outcomes. The development and assessment of computational methods that can treat larger reaction systems are also future tasks. Considering the limitations of DFT calculations, the development of empirical activity descriptors that can be easily measured by experiments and effectively predict the activities of nanozymes is also desirable. Because most nanozymes have weak substrate specificity, the design of new nanozymes with improved substrate specificity based on the catalytic mechanisms and kinetics is a future challenge. Besides catalytic activities, the mechanisms of the other fundamental properties of nanozymes, for example, their in vivo transportation, degradation, and toxicities, which are closely relevant to the therapeutic effects of nanozymes, deserve particular attention in the future.

Acknowledgements

This work was supported by the National Natural Science Foundation of China (NSFC) (Project No. 22007041) and Natural Science Foundation of Jiangxi Province (Project No. 20211BAB213019).

Conflict of Interest

The authors declare no conflict of interest.

Keywords

density functional theory calculations, heterogeneous catalysis, inorganic nanomaterials, oxidordeuctases, structure–activity relationship

Received: November 30, 2022
Revised: December 28, 2022
Published online:

[1] F. Manea, F. B. Houillon, L. Pasquato, P. Scrimin, *Angew. Chem., Int. Ed.* **2004**, *43*, 6165.
[2] L. Gao, J. Zhuang, L. Nie, J. Zhang, Y. Zhang, N. Gu, T. Wang, J. Feng, D. Yang, S. Perrett, X. Yan, *Nat. Nanotechnol.* **2007**, *2*, 577.

© 2023 Wiley-VCH GmbH

15214095, 0, Downloaded from https://onlinelibrary.wiley.com/doi/10.1002/adma.202211151 by Eth Zürich Eth-Bibliothek, Wiley Online Library on [11/07/2023]. See the Terms and Conditions (https://onlinelibrary.wiley.com/terms-and-conditions) on Wiley Online Library for rules of use; OA articles are governed by the applicable Creative Commons License

[3] H. Wei, E. Wang, *Chem. Soc. Rev.* **2013**, *42*, 6060.
[4] a) C. Korsvik, S. Patil, S. Seal, W. T. Self, *Chem. Commun.* **2007**, 1056; b) S. S. Ali, J. I. Hardt, L. L. Dugan, *Nanomedicine* **2008**, *4*, 283.
[5] K. Yokota, I. Yamazaki, *Biochem. Biophys. Res. Commun.* **1965**, *18*, 48.
[6] F. Attar, M. G. Shahpar, B. Rasti, M. Sharifi, A. A. Saboury, S. M. Rezayat, M. Falahati, *J. Mol. Liq.* **2019**, *278*, 130.
[7] A. Najafi, M. Keykhaee, H. Khorramdelazad, M. Y. Karimi, L. N. Samimi, N. Aghamohamadi, M. Karimi, R. Falak, M. Khoobi, *Biomed. Pharmacother.* **2022**, *153*, 113483.
[8] Y. Chong, Q. Liu, C. Ge, *Nano Today* **2021**, *37*, 101076.
[9] H. Zhao, R. Zhang, X. Yan, K. Fan, *J. Mater. Chem. B* **2021**, *9*, 6939.
[10] L.-W. Xia, L. Ding, M.-L. Chen, Y. Jiao, Y.-H. Cheng, Z. Xu, *Shengwu Huaxue Yu Shengwu Wuli Jinzhan* **2021**, *48*, 24.
[11] Z. Zhang, L. M. Bragg, M. R. Servos, J. Liu, *Chin. Chem. Lett.* **2019**, *30*, 1655.
[12] a) D. Duan, K. Fan, D. Zhang, S. Tan, M. Liang, Y. Liu, J. Zhang, P. Zhang, W. Liu, X. Qiu, G. P. Kobinger, G. F. Gao, X. Yan, *Biosens. Bioelectron.* **2015**, *74*, 134; b) T. Zhang, F. Tian, L. Long, J. Liu, X. Wu, *Int. J. Nanomed.* **2018**, *13*, 4795; c) A. Li, L. Long, F. Liu, J. Liu, X. Wu, Y. Ji, *J. Biol. Eng.* **2019**, *13*, 87.
[13] a) J. Han, J. Yoon, *ACS Appl. Bio Mater.* **2020**, *3*, 7344; b) Y. Yang, D. Zhu, Y. Liu, B. Jiang, W. Jiang, X. Yan, K. Fan, *Nanoscale* **2020**, *12*, 13548; c) X. Meng, D. Li, L. Chen, H. He, Q. Wang, C. Hong, J. He, X. Gao, Y. Yang, B. Jiang, G. Nie, X. Yan, L. Gao, K. Fan, *ACS Nano* **2021**, *15*, 5735; d) C. Cao, N. Yang, Y. Su, Z. Zhang, C. Wang, X. Song, P. Chen, W. Wang, X. Dong, *Adv. Mater.* **2022**, *34*, 2203236.
[14] a) Y. Meng, W. Li, X. Pan, G. M. Gadd, *Environ. Sci.: Nano* **2020**, *7*, 1305; b) C. Hong, X. Meng, J. He, K. Fan, X. Yan, *Particuology* **2022**, *71*, 90.
[15] a) A. R. H. Jangi, M. R. H. Jangi, S. R. H. Jangi, *Chin. J. Chem. Eng.* **2020**, *28*, 1492; b) N. Stasyuk, O. Smutok, O. Demkiv, T. Prokopiv, G. Gayda, M. Nisnevitch, M. Gonchar, *Sensors* **2020**, *20*, 4509; c) Y. Huang, J. Ren, X. Qu, *Chem. Rev.* **2019**, *119*, 4357; d) D. Xu, L. Wu, H. Yao, L. Zhao, *Small* **2022**, *18*, 2203400; e) H. Wang, K. Wan, X. Shi, *Adv. Mater.* **2019**, *31*, 1805368.
[16] a) S. Zhao, H. Duan, Y. Yang, X. Yan, K. Fan, *Nano Lett.* **2019**, *19*, 8887; b) H. Song, C. Ma, L. Wang, Z. Zhu, *Nanoscale* **2020**, *12*, 19284; c) G. Wang, J. Wei, R. Hu, L. Mei, A. Wan, J. Feng, *Biosens. Bioelectron.* **2022**, *215*, 114552; d) Z. Zhu, H. Luo, T. Wang, C. Zhang, M. Liang, D. Yang, M. Liu, W. W. Yu, Q. Bai, L. Wang, N. Sui, *Chem. Mater.* **2022**, *34*, 1356.
[17] a) S. Hu, C. Yang, Y. Li, Q. Luo, H. Luo, *Biosens. Bioelectron.* **2022**, *199*, 113881; b) X. Mu, H. He, J. Wang, W. Long, Q. Li, H. Liu, Y. Gao, L. Ouyang, Q. Ren, S. Sun, J. Wang, J. Yang, Q. Liu, Y. Sun, C. Liu, X.-D. Zhang, W. Hu, *Nano Lett.* **2019**, *19*, 4527; c) X. Mu, J. Wang, Y. Li, F. Xu, W. Long, L. Ouyang, H. Liu, Y. Jing, J. Wang, H. Dai, Q. Liu, Y. Sun, C. Liu, X. Zhang, *ACS Nano* **2019**, *13*, 1870; d) Y. Li, R. Fu, Z. Duan, C. Zhu, D. Fan, *Adv. Healthcare Mater.* **2022**, *11*, 2101849.
[18] a) R. Karaman, *Chem. Biol. Drug Des.* **2013**, *82*, 643; b) G. Longhi, E. Castiglioni, J. Koshoubu, G. Mazzeo, S. Abbate, *Chirality* **2016**, *28*, 696; c) C. Fu, C. Liu, T. Li, X. Zhang, F. Wang, J. Yang, Y. Jiang, P. Cui, H. Li, *Comput. Mater. Sci.* **2019**, *170*, 109202; d) A. H. Mazurek, L. Szeleszczuk, D. M. Pisklak, *Pharmaceutics* **2020**, *12*, 415; e) P. Makkar, N. N. Ghosh, *RSC Adv.* **2021**, *11*, 27897.
[19] a) S. S. Ali, J. I. Hardt, K. L. Quick, J. S. Kim-Han, B. F. Erlanger, T. T. Huang, C. J. Epstein, L. L. Dugan, *Free Radical Biol. Med.* **2004**, *37*, 1191; b) H. Sun, A. Zhao, N. Gao, K. Li, J. Ren, X. Qu, *Angew. Chem., Int. Ed.* **2015**, *54*, 7176.
[20] I. Czekaj, J. Wambach, O. Krocher, *Int. J. Mol. Sci.* **2009**, *10*, 4310.
[21] J.-X. Liu, W.-X. Li, *Comput. Mol. Sci.* **2016**, *6*, 571.
[22] S. Rinaldi, M. W. Van der Kamp, K. E. Ranaghan, A. J. Mulholland, G. Colombo, *ACS Catal.* **2018**, *8*, 5698.
[23] M. J. Frisch, G. W. Trucks, H. B. Schlegel, G. E. Scuseria, M. A. Robb, J. R. Cheeseman, G. Scalmani, V. Barone, G. A. Petersson, H. Nakatsuji, X. Li, M. Caricato, A. V. Marenich, J. Bloino, B. G. Janesko, R. Gomperts, B. Mennucci, H. P. Hratchian, J. V. Ortiz, A. F. Izmaylov, J. L. Sonnenberg, F. D. Williams, F. Lipparini, F. Egidi, J. Goings, B. Peng, A. Petrone, T. Henderson, D. Ranasinghe, V. G. Zakrzewski, et al., Wallingford CT, USA **2016**.
[24] M. W. Schmidt, K. K. Baldridge, J. A. Boatz, S. T. Elbert, M. S. Gordon, J. H. Jensen, S. Koseki, N. Matsunaga, K. A. Nguyen, S. Su, T. L. Windus, M. Dupuis, J. A. Montgomery Jr., *J. Comput. Chem.* **1993**, *14*, 1347.
[25] a) G. Kresse, J. Furthmuller, *Phys. Rev. B* **1996**, *54*, 11169; b) G. Kresse, J. Furthmüller, *Comput. Mater. Sci.* **1996**, *6*, 15.
[26] S. J. Clark, M. D. Segall, C. J. Pickard, P. J. Hasnip, M. I. J. Probert, K. Refson, M. C. Payne, *Z. Kristallogr.* **2005**, *220*, 567.
[27] a) Y.-G. Wang, D. Mei, J. Li, R. Rousseau, *J. Phys. Chem.* **2013**, *117*, 23082; b) T. Fujitani, I. Nakamura, A. Takahashi, *ACS Catal.* **2020**, *10*, 2517.
[28] a) S. Lutz, I. Tubert-Brohman, Y. Yang, M. Meuwly, *J. Biol. Chem.* **2011**, *286*, 23679; b) E. Codorniu-Hernandez, P. G. Kusalik, *J. Am. Chem. Soc.* **2012**, *134*, 532; c) H. Li, F. Xie, M.-T. Zhang, *ACS Catal.* **2021**, *11*, 68.
[29] a) S. J. Hong, H. Chun, M. Hong, B. Han, *Appl. Surf. Sci.* **2022**, *598*, 153715; b) Q.-Z. Li, H. Fan, Z. Wang, J.-J. Zheng, K. Fan, X. Yan, X. Gao, *ACS Catal.* **2022**, *13*, 504.
[30] X. Zhang, Q. Yang, Y. Lang, X. Jiang, P. Wu, *Anal. Chem.* **2020**, *92*, 12400.
[31] Y. Misono, Y. Ohkata, T. Morikawa, K. Itoh, *J. Electroanal. Chem.* **1997**, *436*, 203.
[32] a) H. Wei, E. Wang, *Anal. Chem.* **2008**, *80*, 2250; b) W. W. He, X. C. Wu, J. B. Liu, X. N. Hu, K. Zhang, S. A. Hou, W. Y. Zhou, S. S. Xie, *Chem. Mater.* **2010**, *22*, 2988; c) Y. Song, K. Qu, C. Zhao, J. Ren, X. Qu, *Adv. Mater.* **2010**, *22*, 2206; d) H. Zhao, Y. Dong, P. Jiang, G. Wang, J. Zhang, *ACS Appl. Mater. Interfaces* **2015**, *7*, 6451.
[33] a) Y. Jv, B. X. Li, R. Cao, *Chem. Commun.* **2010**, *46*, 8017; b) G. Fang, W. Li, X. Shen, J. M. Perez-Aguilar, Y. Chong, X. Gao, Z. Chai, C. Chen, C. Ge, R. Zhou, *Nat. Commun.* **2018**, *9*, 129; c) G. Jin, J. Liu, C. Wang, W. Gu, G. Ran, B. Liu, Q. Song, *Appl. Catal., B* **2020**, *267*, 118725; d) Z. Xi, K. Wei, Q. Wang, M. J. Kim, S. Sun, V. Fung, X. Xia, *J. Am. Chem. Soc.* **2021**, *143*, 2660.
[34] Y. Zhao, S. Zhuang, L. Liao, C. Wang, N. Xia, Z. Gan, W. Gu, J. Li, H. Deng, Z. Wu, *J. Am. Chem. Soc.* **2020**, *142*, 973.
[35] H. Liu, Y. Li, S. Sun, Q. Xin, S. Liu, X. Mu, X. Yuan, K. Chen, H. Wang, K. Varga, W. Mi, J. Yang, X. D. Zhang, *Nat. Commun.* **2021**, *12*, 114.
[36] a) Z. Tian, J. Li, Z. Zhang, W. Gao, X. Zhou, Y. Qu, *Biomaterials* **2015**, *59*, 116; b) Y. Yang, Z. Mao, W. Huang, L. Liu, J. Li, J. Li, Q. Wu, *Sci. Rep.* **2016**, *6*, 35344; c) S. Singh, T. Dosani, A. S. Karakoti, A. Kumar, S. Seal, W. T. Self, *Biomaterials* **2011**, *32*, 6745.
[37] a) D. Jampaiah, T. S. Reddy, A. E. Kandjani, P. R. Selvakannan, Y. M. Sabri, V. E. Coyle, R. Shukla, S. K. Bhargava, *J. Mater. Chem. B* **2016**, *4*, 3874; b) W. Guo, M. Zhang, Z. Lou, M. Zhou, P. Wang, H. Wei, *ChemCatChem* **2019**, *11*, 737.
[38] a) R. André, F. Natálio, M. Humanes, J. Leppin, K. Heinze, R. Wever, H. C. Schröder, W. E. G. Müller, W. Tremel, *Adv. Funct. Mater.* **2011**, *21*, 501; b) S. Ghosh, P. Roy, N. Karmodak, E. D. Jemmis, G. Mugesh, *Angew. Chem., Int. Ed.* **2018**, *57*, 4510.
[39] a) S. Liu, F. Lu, R. Xing, J. J. Zhu, *Chemistry* **2011**, *17*, 620; b) K. Fan, H. Wang, J. Xi, Q. Liu, X. Meng, D. Duan, L. Gao, X. Yan, *Chem. Commun.* **2017**, *53*, 424.
[40] J. Mu, L. Zhang, G. Zhao, Y. Wang, *Phys. Chem. Chem. Phys.* **2014**, *16*, 15709.
[41] S. K. Warkhade, R. P. Singh, R. S. Das, G. S. Gaikwad, S. P. Zodape, U. R. Pratap, A. Maldhure, A. V. Wankhade, *Inorg. Chem. Commun.* **2021**, *126*, 108461.

© 2023 Wiley-VCH GmbH

15214095, 0, Downloaded from https://onlinelibrary.wiley.com/doi/10.1002/adma.202211151 by Eth Zürich Eth-Bibliothek, Wiley Online Library on [11/07/2023]. See the Terms and Conditions (https://onlinelibrary.wiley.com/terms-and-conditions) on Wiley Online Library for rules of use; OA articles are governed by the applicable Creative Commons License

[42] F. Cao, L. Zhang, H. Wang, Y. You, Y. Wang, N. Gao, J. Ren, X. Qu, *Angew. Chem., Int. Ed.* **2019**, *58*, 16236.
[43] Y. Zhang, S. Yang, J. Wang, Y. Cai, L. Niu, X. Liu, C. Liu, H. Qi, A. Liu, *Talanta* **2021**, *233*, 122594.
[44] R. Zhao, X. Zhao, X. Gao, *Chem. - Eur. J.* **2015**, *21*, 960.
[45] B. Xie, X. Yang, R. Zhang, J. Guo, Z. Chen, Y. He, *Sens. Actuators, B* **2021**, *347*,130597.
[46] Y. Wang, G. Jia, X. Cui, X. Zhao, Q. Zhang, L. Gu, L. Zheng, L. H. Li, Q. Wu, D. J. Singh, D. Matsumura, T. Tsuji, Y.-T. Cui, J. Zhao, W. Zheng, *Chem* **2021**, *7*, 436.
[47] J. Wu, X. Wang, Q. Wang, Z. Lou, S. Li, Y. Zhu, L. Qin, H. Wei, *Chem. Soc. Rev.* **2019**, *48*, 1004.
[48] B. Jiang, D. Duan, L. Gao, M. Zhou, K. Fan, Y. Tang, J. Xi, Y. Bi, Z. Tong, G. F. Gao, N. Xie, A. Tang, G. Nie, M. Liang, X. Yan, *Nat. Protoc.* **2018**, *13*, 1506.
[49] D. Peak, J. W. J. P. R. B. Corbett, *Phys. Rev. B* **1972**, *5*, 1226.
[50] J. Dong, L. Song, J. J. Yin, W. He, Y. Wu, N. Gu, Y. Zhang, *ACS Appl. Mater. Interfaces* **2014**, *6*, 1959.
[51] H. J. H. Fenton, *J. Chem. Soc.* **1894**, *65*, 899.
[52] M. Ma, Y. Zhang, N. Gu, *Colloids Surf., A* **2011**, *373*, 6.
[53] P. Borthakur, P. K. Boruah, M. R. Das, *ACS Sustainable Chem. Eng.* **2021**, *9*, 13245.
[54] J. Chen, Q. Wang, L. Huang, H. Zhang, K. Rong, H. Zhang, S. Dong, *Nano Res.* **2018**, *11*, 4905.
[55] S. Y. Yin, G. Song, Y. Yang, Y. Zhao, P. Wang, L. M. Zhu, X. Yin, X. B. Zhang, *Adv. Funct. Mater.* **2019**, *29*, 1901417.
[56] M. Chang, M. Wang, M. Wang, M. Shu, B. Ding, C. Li, M. Pang, S. Cui, Z. Hou, J. Lin, *Adv. Mater.* **2019**, *31*, 1905271.
[57] D. R. Hang, Y. Q. Pan, K. H. Sharma, M. M. C. Chou, S. E. Islam, H. F. Wu, C. T. Liang, *Nanomaterial* **2020**, *10*, 2045.
[58] Z. W. Chen, J. J. Yin, Y. T. Zhou, Y. Zhang, L. Song, M. J. Song, S. L. Hu, N. Gu, *ACS Nano* **2012**, *6*, 4001.
[59] W. Zhu, N. Hao, J. Lu, Z. Dai, J. Qian, X. Yang, K. Wang, *Chem. Commun.* **2020**, *56*, 1409.
[60] J. Li, W. Liu, X. Wu, X. Gao, *Biomaterials* **2015**, *48*, 37.
[61] Z. Wang, X. Shen, X. Gao, *J. Phys. Chem. C* **2021**, *125*, 23098.
[62] Y. Hu, X. J. Gao, Y. Zhu, F. Muhammad, S. Tan, W. Cao, S. Lin, Z. Jin, X. Gao, H. Wei, *Chem. Mater.* **2018**, *30*, 6431.
[63] X. Shen, Z. Wang, X. Gao, Y. Zhao, *ACS Catal.* **2020**, *10*, 12657.
[64] a) Z. Z. Wang, X. M. Shen, X. F. Gao, Y. L. Zhao, *Nanoscale* **2019**, *11*, 13289; b) Z. Wang, J. Wu, J. J. Zheng, X. Shen, L. Yan, H. Wei, X. Gao, Y. Zhao, *Nat. Commun.* **2021**, *12*, 6866.
[65] L. Zhao, R. He, K. T. Rim, T. Schiros, K. S. Kim, H. Zhou, C. Gutierrez, S. P. Chockalingam, C. J. Arguello, L. Palova, D. Nordlund, M. S. Hybertsen, D. R. Reichman, T. F. Heinz, P. Kim, A. Pinczuk, G. W. Flynn, A. N. Pasupathy, *Science* **2011**, *333*, 999.
[66] R. S. D. Guo, C. Akiba, S. Saji, T. Kondo, J. Nakamura, *Science* **2016**, *351*, 361.
[67] L. K. Putri, W.-J. Ong, W. S. Chang, S.-P. Chai, *Appl. Surf. Sci.* **2015**, *358*, 2.
[68] D. Wang, X. Song, P. Li, X. J. Gao, X. Gao, *J. Mater. Chem. B* **2020**, *8*, 9028.
[69] Q. Liang, J. Xi, X. J. Gao, R. Zhang, Y. Yang, X. Gao, X. Yan, L. Gao, K. Fan, *Nano Today* **2020**, *35*, 100935.
[70] X. J. Gao, J. Yan, J.-J. Zheng, S. Zhong, X. Gao, *Adv. Healthcare Mater.* **2023**, 2202925.
[71] J. Greeley, I. E. Stephens, A. S. Bondarenko, T. P. Johansson, H. A. Hansen, T. F. Jaramillo, J. Rossmeisl, I. Chorkendorff, J. K. Norskov, *Nat. Chem.* **2009**, *1*, 552.
[72] M. Fumanal, G. Capano, S. Barthel, B. Smit, I. Tavernelli, *J. Mater. Chem. A* **2020**, *8*, 4473.
[73] P. Sabatier, *Ber. Dtsch. Chem. Ges.* **1911**, *44*, 1984.
[74] F. H. B. Lima, J. Zhang, M. H. Shao, K. Sasaki, M. B. Vukmirovic, E. A. Ticianelli, R. R. Adzic, *J. Phys. Chem. C* **2007**, *111*, 404.
[75] J. Suntivich, K. J. May, H. A. Gasteiger, J. B. Goodenough, Y. Shao-Horn, *Science* **2011**, *334*, 1383.
[76] X. Wang, X. J. Gao, L. Qin, C. Wang, L. Song, Y. N. Zhou, G. Zhu, W. Cao, S. Lin, L. Zhou, K. Wang, H. Zhang, Z. Jin, P. Wang, X. Gao, H. Wei, *Nat. Commun.* **2019**, *10*, 704.
[77] X. Shen, W. Liu, X. Gao, Z. Lu, X. Wu, X. Gao, *J. Am. Chem. Soc.* **2015**, *137*, 15882.
[78] Y. Chen, X. Shen, U. Carmona, F. Yang, X. Gao, M. Knez, L. Zhang, Y. Qin, *Adv. Mater. Interfaces* **2021**, *8*, 2100086.
[79] L. Jiao, J. Wu, H. Zhong, Y. Zhang, W. Xu, Y. Wu, Y. Chen, H. Yan, Q. Zhang, W. Gu, L. Gu, S. P. Beckman, L. Huang, C. Zhu, *ACS Catal.* **2020**, *10*, 6422.
[80] Z. Wei, P. Sautet, *Angew. Chem., Int. Ed.* **2022**, *61*, e202210060.
[81] Y. Fan, X. Gan, H. Zhao, Z. Zeng, W. You, X. Quan, *Chem. Eng. J.* **2022**, *427*, 131572.
[82] S. Ji, B. Jiang, H. Hao, Y. Chen, J. Dong, Y. Mao, Z. Zhang, R. Gao, W. Chen, R. Zhang, Q. Liang, H. Li, S. Liu, Y. Wang, Q. Zhang, L. Gu, D. Duan, M. Liang, D. Wang, X. Yan, Y. Li, *Nat. Catal.* **2021**, *4*, 407.
[83] T. Wang, Q. Bai, Z. Zhu, H. Xiao, F. Jiang, F. Du, W. W. Yu, M. Liu, N. Sui, *Chem. Eng. J.* **2021**, *413*, 127537.
[84] F. Natalio, R. Andre, A. F. Hartog, B. Stoll, K. P. Jochum, R. Wever, W. Tremel, *Nat. Nanotechnol.* **2012**, *7*, 530.
[85] A. Asati, S. Santra, C. Kaittanis, S. Nath, J. M. Perez, *Angew. Chem., Int. Ed.* **2009**, *48*, 2308.
[86] Y. Peng, X. Chen, G. Yi, Z. Gao, *Chem. Commun.* **2011**, *47*, 2916.
[87] H. J. Cheng, S. C. Lin, F. Muhammad, Y. W. Lin, H. Wei, *ACS Sens.* **2016**, *1*, 1336.
[88] L. Jiang, S. Fernandez-Garcia, M. Tinoco, Z. X. Yan, Q. Xue, G. Blanco, J. J. Calvino, A. B. Hungria, X. W. Chen, *ACS Appl. Mater. Interfaces* **2017**, *9*, 18595.
[89] a) Z. Yuan, X. Liu, J. Ling, G. Huang, J. Huang, X. Zhu, L. He, T. Chen, *Biomaterials* **2022**, *287*, 121620; b) X. Zhang, Y. Huang, *Anal. Methods* **2015**, *7*, 8640.
[90] Y. Wu, L. Jiao, X. Luo, W. Xu, X. Wei, H. Wang, H. Yan, W. Gu, B. Z. Xu, D. Du, Y. Lin, C. Zhu, *Small* **2019**, *15*, 1903108.
[91] Y. Ai, H. Sun, Z. Gao, C. Wang, L. Guan, Y. Wang, Y. Wang, H. Zhang, Q. Liang, *Adv. Funct. Mater.* **2021**, *31*, 2103581.
[92] S.-B. He, L. Yang, M.-T. Lin, H. A. A. Noreldeen, R.-X. Yu, H.-P. Peng, H.-H. Deng, W. Chen, *Sens. Actuators, B* **2021**, *347*, 130627.
[93] Y. Zhu, W. Wang, J. Cheng, Y. Qu, Y. Dai, M. Liu, J. Yu, C. Wang, H. Wang, S. Wang, C. Zhao, Y. Wu, Y. Liu, *Angew. Chem., Int. Ed.* **2021**, *60*, 9480.
[94] X. Wang, F. Wen, L. He, J. Su, P. Jiang, D. He, *Anal. Chim. Acta* **2022**, *1198*, 339564.
[95] R. Wu, M. Sun, X. Liu, F. Qin, X. Zhang, Z. Qian, J. Huang, Y. Li, T. Tan, W. Chen, Z. Chen, *Anal. Chem.* **2022**, *94*, 14308.
[96] P. Cheng, H. Wang, X. Shi, *Nanoscale* **2020**, *12*, 3050.
[97] K. Zhang, X. N. Hu, J. B. Liu, J. J. Yin, S. A. Hou, T. Wen, W. W. He, Y. L. Ji, Y. T. Guo, Q. Wang, X. C. Wu, *Langmuir* **2011**, *27*, 2796.
[98] J. Chen, Q. Ma, M. Li, D. Chao, L. Huang, W. Wu, Y. Fang, S. Dong, *Nat. Commun.* **2021**, *12*, 3375.
[99] J. Wu, Z. Wang, X. Jin, S. Zhang, T. Li, Y. Zhang, H. Xing, Y. Yu, H. Zhang, X. Gao, H. Wei, *Adv. Mater.* **2020**, *33*, 2005024.
[100] C. Ge, G. Fang, X. Shen, Y. Chong, W. G. Wamer, X. Gao, Z. Chai, C. Chen, J.-J. Yin, *ACS Nano* **2016**, *10*, 10436.
[101] M. Zhu, Y. Wen, S. Song, A. Zheng, J. Li, W. Sun, Y. Dai, K. Yin, L. Sun, *Nanoscale* **2020**, *12*, 19104.
[102] G. F. Liu, M. Filipovic, I. Ivanovic-Burmazovic, F. Beuerle, P. Witte, A. Hirsch, *Angew. Chem., Int. Ed.* **2008**, *47*, 3991.
[103] A. Djordjevic, G. Bogdanovic, *Arch. Oncol.* **2008**, *16*, 42.
[104] I. Celardo, J. Z. Pedersen, E. Traversa, L. Ghibelli, *Nanoscale* **2011**, *3*, 1411.
[105] Z. Wang, X. Shen, X. Gao, Y. Zhao, *Nanoscale* **2019**, *11*, 13289.
[106] S. Osuna, M. Swart, M. Sola, *Chem. - Eur. J.* **2010**, *16*, 3207.

© 2023 Wiley-VCH GmbH

15214095, 0, Downloaded from https://onlinelibrary.wiley.com/doi/10.1002/adma.202211151 by Eth Zürich Eth-Bibliothek, Wiley Online Library on [11/07/2023]. See the Terms and Conditions (https://onlinelibrary.wiley.com/terms-and-conditions) on Wiley Online Library for rules of use; OA articles are governed by the applicable Creative Commons License

[107] a) Z. Wang, S. Wang, Z. Lu, X. Gao, *J. Cluster Sci.* **2015**, *26*, 375; b) Z. Wang, X. Gao, Y. Zhao, *J. Phys. Chem. A* **2018**, *122*, 8183.
[108] a) J. Mu, X. Zhao, J. Li, E.-C. Yang, X.-J. Zhao, *J. Mater. Chem. B* **2016**, *4*, 5217; b) T. Chen, H. Zou, X. Wu, C. Liu, B. Situ, L. Zheng, G. Yang, *ACS Appl. Mater. Interfaces* **2018**, *10*, 12453; c) N. Singh, M. A. Savanur, S. Srivastava, P. D'Silva, G. Mugesh, *Angew. Chem., Int. Ed.* **2017**, *56*, 14267; d) J. Yao, Y. Cheng, M. Zhou, S. Zhao, S. Lin, X. Wang, J. Wu, S. Li, H. Wei, *Chem. Sci.* **2018**, *9*, 2927; e) N. Singh, M. Geethika, S. M. Eswarappa, G. Mugesh, *Chem. - Eur. J.* **2018**, *24*, 8393.
[109] S. Haastrup, M. Strange, M. Pandey, T. Deilmann, P. S. Schmidt, N. F. Hinsche, M. N. Gjerding, D. Torelli, P. M. Larsen, A. C. Riis-Jensen, J. Gath, K. W. Jacobsen, J. J. Mortensen, T. Olsen, K. S. Thygesen, *2D Mater.* **2018**, *5*, 042002.
[110] a) T. Pirmohamed, J. M. Dowding, S. Singh, B. Wasserman, E. Heckert, A. S. Karakoti, J. E. King, S. Seal, W. T. Self, *Chem. Commun.* **2010**, *46*, 2736; b) V. Nicolini, E. Gambuzzi, G. Malavasi, L. Menabue, M. C. Menziani, G. Lusvardi, A. Pedone, F. Benedetti, P. Luches, S. D'Addato, S. Valeri, *J. Phys. Chem. B* **2015**, *119*, 4009.
[111] H. Deng, W. Shen, Y. Peng, X. Chen, G. Yi, Z. Gao, *Chem. - Eur. J.* **2012**, *18*, 8906.
[112] a) J. Mu, L. Zhang, M. Zhao, Y. Wang, *J. Mol. Catal. A: Chem.* **2013**, *378*, 30; b) J. Mu, L. Zhang, M. Zhao, Y. Wang, *ACS Appl. Mater. Interfaces* **2014**, *6*, 7090.
[113] J. Liu, L. Wang, X. Shen, X. Gao, Y. Chen, H. Liu, Y. Liu, D. Yin, Y. Liu, W. Xu, R. Cai, M. You, M. Guo, Y. Wang, J. Li, Y. Li, C. Chen, *Nano Today* **2020**, *34*, 100907.
[114] R. Zhang, L. Chen, Q. Liang, J. Xi, H. Zhao, Y. Jin, X. Gao, X. Yan, L. Gao, K. Fan, *Nano Today* **2021**, *41*, 101317.
[115] X. Zhang, S. Zhang, Z. Yang, Z. Wang, X. Tian, R. Zhou, *Nanoscale* **2021**, *13*, 12613.
[116] W. He, Y.-T. Zhou, W. G. Wamer, M. D. Boudreau, J.-J. Yin, *Biomaterials* **2012**, *33*, 7547.
[117] Z. Z. Wang, X. M. Shen, X. F. Gao, Y. L. Zhao, *Nanoscale* **2019**, *11*, 13289.
[118] C. Gu, X. Kong, S. Yan, P. Gai, F. Li, *ACS Sustainable Chem. Eng.* **2020**, *8*, 16549.
[119] M. Gao, Z. Wang, H. Zheng, L. Wang, S. Xu, X. Liu, W. Li, Y. Pan, W. Wang, X. Cai, R. Wu, X. Gao, R. Li, *Angew. Chem., Int. Ed.* **2020**, *59*, 3618.
[120] A. A. Vernekar, T. Das, G. Mugesh, *Angew. Chem., Int. Ed.* **2016**, *55*, 1412.
[121] a) H. Chen, P. Liao, M. L. Mendonca, R. Q. Snurr, *J. Phys. Chem. C* **2018**, *122*, 12362; b) H. Chen, R. Q. Snurr, *ACS Appl. Mater. Interfaces* **2020**, *12*, 14631.
[122] S.-Y. Moon, Y. Liu, J. T. Hupp, O. K. Farha, *Angew. Chem., Int. Ed.* **2015**, *54*, 6795.
[123] M. J. Katz, J. E. Mondloch, R. K. Totten, J. K. Park, S. T. Nguyen, O. K. Farha, J. T. Hupp, *Angew. Chem., Int. Ed.* **2014**, *53*, 497.
[124] T. Islamoglu, A. Atilgan, S.-Y. Moon, G. W. Peterson, J. B. DeCoste, M. Hall, J. T. Hupp, O. K. Farha, *Chem. Mater.* **2017**, *29*, 2672.
[125] S. Y. Moon, Y. Liu, J. T. Hupp, O. K. Farha, *Angew. Chem., Int. Ed.* **2015**, *54*, 6795.
[126] M. R. Momeni, C. J. Cramer, *J. Phys. Chem. C* **2019**, *123*, 15157.
[127] H. Dong, W. Du, J. Dong, R. Che, F. Kong, W. Cheng, M. Ma, N. Gu, Y. Zhang, *Nat. Commun.* **2022**, *13*, 5365.
[128] a) W. Nabi, A. Bansal, B. Xu, *Echocardiography* **2021**, *38*, 982; b) A. S. Makhmet, M. G. Sharaev, A. E. Dyusembaev, A. M. Kustubayeva, *Int. J. Biol.* **2021**, *14*, 4; c) M.-Y. You, A.-N. Lu, Y.-X. Ye, K. Huang, B. Jiang, *Math. Probl. Eng.* **2020**, *2020*, 8345413; d) D. T. Pham, A. A. Afify, *Proc. Inst. Mech. Eng., Part B* **2005**, *219*, 395.
[129] S. Li, Z. Zhou, Z. Tie, B. Wang, M. Ye, L. Du, R. Cui, W. Liu, C. Wan, Q. Liu, S. Zhao, Q. Wang, Y. Zhang, S. Zhang, H. Zhang, Y. Du, H. Wei, *Nat. Commun.* **2022**, *13*, 827.
[130] Y. Wei, J. Wu, Y. Wu, H. Liu, F. Meng, Q. Liu, A. C. Midgley, X. Zhang, T. Qi, H. Kang, R. Chen, D. Kong, J. Zhuang, X. Yan, X. Huang, *Adv. Mater.* **2022**, *34*, 2201736.
[131] J. Razlivina, N. Serov, O. Shapovalova, V. Vinogradov, *Small* **2022**, *18*, e2105673.
[132] C. Zhang, Y. Yu, S. Shi, M. Liang, D. Yang, N. Sui, W. W. Yu, L. Wang, Z. Zhu, *Nano Lett.* **2022**, *22*, 8592.
[133] Y. Yu, Y. Jiang, C. Zhang, Q. Bai, F. Fu, S. Li, L. Wang, W. W. Yu, N. Sui, Z. Zhu, *ACS Mater. Lett.* **2022**, *4*, 2134.

Xiaomei Shen joined Jiangxi Normal University as a Lecturer after she received her Ph.D. degree from Jiangxi Normal University under the supervision of Professor Xingfa Gao in 2019. Her research focuses on density functional theory study of the mechanisms, catalytic reaction kinetics, structure–activity relationship, and design of enzyme-mimetic nanomaterials.

© 2023 Wiley-VCH GmbH

15214095, 0, Downloaded from https://onlinelibrary.wiley.com/doi/10.1002/adma.202211151 by Eth Zürich Eth-Bibliothek, Wiley Online Library on [11/07/2023]. See the Terms and Conditions (https://onlinelibrary.wiley.com/terms-and-conditions) on Wiley Online Library for rules of use; OA articles are governed by the applicable Creative Commons License

Zhenzhen Wang obtained her Ph.D. from Institute of High Energy Physics, Chinese Academy of Science in 2019. Thereafter, she worked in the group of Prof. Xingfa Gao in a Post-Doctoral position. Her research interests include electronic structure, catalytic mechanism, and toxic mechanism of nanomaterials with first-principle calculations and molecular dynamics methods.

Xuejiao J. Gao joined Jiangxi Normal University as a Lecturer after she graduated from the University of Chinese Academy of Sciences in 2017 with a Ph.D. Her research interests are theoretical calculation of surface and interface chemistry of nanomaterials. She uses first-principles methods to study the mechanism, catalytic reaction kinetics, structure–activity relationship, and theoretical model of the activation of H_2O_2 by nanomaterials. Also, she is interested in the machine-learning-guided design and prediction of functional nanomaterials targeting biomedical applications, including tumor therapy and antibacterial.

Xingfa Gao is a Professor and Principal Investigator at National Center for Nanoscience and Technology of China. He obtained his Ph.D. from Institute of High Energy Physics, Chinese Academy of Science under the supervision of Professor Yuliang Zhao in 2006. He moved to the Institute for Molecular Science, Japan as a Postdoctoral Fellow with Prof. Shigeru Nagase (2006–2010) and Rensselaer Polytechnic Institute, USA as a Postdoctoral Fellow with Prof. Shengbai Zhang (2010–2011). His research interest includes the theory and computation of nano–bio interactions and the computer-aided design of nanomedicine.

© 2023 Wiley-VCH GmbH

15214095, 0, Downloaded from https://onlinelibrary.wiley.com/doi/10.1002/adma.202211151 by Eth Zürich Eth-Bibliothek, Wiley Online Library on [11/07/2023]. See the Terms and Conditions (https://onlinelibrary.wiley.com/terms-and-conditions) on Wiley Online Library for rules of use; OA articles are governed by the applicable Creative Commons License